Mechanical Properties and Characterization of Nanocrystalline Ni and Ni Solid Solutions

Thesis by
Miranda Lee Schwacke

In Partial Fulfillment of the Requirements for the
Degree of
Bachelor of Science

CALIFORNIA INSTITUTE OF TECHNOLOGY
Pasadena, California

2020
Submitted May 29, 2020

ACKNOWLEDGEMENTS

I'd like to thank my thesis advisor, Professor Julia Greer, as well as my mentor (and the other half of the Andas) Amanda Mattsson. I'd also like to thank Daryl Yee and Rebecca Gallivan for their guidance and assistance with fabricating and testing samples, as well as the rest of the Greer Group.

ABSTRACT

In this work we investigate the mechanical properties of nanocrystalline Ni and Ni solid solutions made by both traditional fabrication methods (through a literature review) and by a newly developed chemical-derivation method (through experimental characterization and nanoindentaiton testing). Chapter 1 consists of a review of the current literature on nanocrystalline Ni. It focuses specifically on how the grain size of these materials is related to hardness through the Hall-Petch relationship and at grain sizes past the Hall-Petch breakdown. Given the number of apparent deviations from the Hall-Petch relationship found in the literature, in Chapter 2 we consider factors other than grain size which can impact hardness, including additives, annealing, and texture. Chapter 3 provides a description of our own experimental methods and results, including sample fabrication, grain size measurement, and nanoindentation. The hardness and reduced modulus of our nanocrystalline Ni samples are calculated to be 56 MPa and 1.76 GPa, respectively. These values are very low compared to what is described in the literature. Chapter 4 presents models for the hardness and Young's modulus of nanocrystalline materials as functions of porosity, impurity content, and other factors which might cause anomalously low values. However, we find that these models are unable to account for the values we have observed. Chapter 5 includes a discussion of future work which should be done in order to better understand the deformation occuring in chemically-derived nanocrystalline Ni and how it differs from what is described in the literature.

TABLE OF CONTENTS

LIST OF ILLUSTRATIONS

LIST OF TABLES

Chapter 1

INTRODUCTION TO NANOCRYSTALLINE MATERIALS, THE HALL-PETCH EFFECT, AND THE HALL-PETCH BREAKDOWN

Most crystalline solids are not a single monolithic crystal, but are instead composed of many smaller crystallites which vary in size and orientation. These crystallites are called grains, and the interfaces between them are called grain boundaries. Conventional coarse-grained materials typically have grains with average diameters between 10 and 300 μm. However, the observation that materials with smaller grains have many desirable properties, has lead to interest in ultra-fine grained and nanocrystalline materials. Ultra-fine grain size is typically defined as 500 nm to 1 μm, and materials are typically considered nanocrystalline if they have grain sizes between 1 and 500 nm. Nanocrystalline materials can have many advantageous mechanical properties including increased strength and hardness, increased toughness, decreased elastic modulus and ductility, high diffusivity, increased heat capacity, and superior soft magnetic properties [1]. Because of these desirable properties, there has been much interest in nanocrystalline materials both for their potential structural applications and for what can be learned about how fundamental material deformation mechanisms change at small scales.

1.1 The Hall-Petch Effect

It has long been known that the strength of a material increases with decreasing grain size. In the early 1950s Hall and Petch showed empirically that the yield point of steels was related to their grain size, d, following the now well-known Hall-Petch relationship:

$$\sigma_y = \sigma_0 + kd^{-1/2} \tag{1.1}$$

where σ_0 and k are material-dependent constants [2, 3]. Since then, this relationship has been shown to apply to yield stress, flow stress, and hardness of many metals and alloys [4].

Many authors have offered rationales for the mathematical expression of the Hall-Petch relationship. Most models treat the terms σ_0 and $kd^{-1/2}$ separately; $kd^{-1/2}$ is assumed to represent the grain size strengthening physics while σ_0 accounts

for strength unrelated to grain size. According to the model suggested by Hall and Petch, in bulk polycrystalline materials, plastic deformation occurs by the glide of lattice dislocations and their piling up against grain boundaries. Furthermore, macroscopic yielding occurs when dislocations are emitted into adjacent grains. The total length of a dislocation pile-up is limited by the grain size. Decreasing grain size limits the number of dislocations which can pile-up in each grain, which also limits the stress at the head of the pile-up, and thus higher stresses are required for plastic deformation to occur [2, 3]. There are many variations of Hall and Petch's pile-up model which all predict a grain size-strengthening relationship of the form

$$\sigma = \sigma_0 + \beta G b^{1/2} d^{-1/2} \tag{1.2}$$

where b is the magnitude of the Burger's vector, G is the shear modulus, and β is a constant ($\beta \approx 0.18$ on average for FCC metals like Ni) [4].

However, there is no direct evidence which relates dislocation pile-up length to grain size, and the pile-up model fails to account for k dependence on grain boundary structure and chemistry. This has led other authors to develop work-hardening models based on the idea that grain boundaries influence dislocation density which then affects flow stress:

$$\sigma = \sigma_0 + \alpha G b \sqrt{\rho} \tag{1.3}$$

where α is a material dependent constant. For a more extensive summary and discussion of the various models which have been used to explain the Hall-Petch relationship see Cordero et al.'s review [4].

1.2 Breakdown of the Hall-Petch Effect

As the grain size of a material decreases, grain boundaries become an increasing fraction of the overall volume compared to grains. If we assume that grains have a cubic or spherical shape, the volume fraction of grain boundaries can be estimated as $3\Delta/d$ where Δ is the thickness of the grain boundaries and d is the grain diameter [1]. Assuming a grain boundary thickness of 1 nm, for 100 nm grains, the volume fraction of grain boundaries is around 3%. For 5 nm grains the volume fraction of grain boundaries is approximately 50%, which is remarkably higher. Furthermore, the number of dislocations which can fit in a single grain decreases, and at small enough grain sizes grains can no longer fit multiple dislocations. This has significant implications for the mechanical properties of nanocrystalline materials. The Hall-Petch relationship has generally been found to hold for materials until they reach

a grain size of $d \sim 20$ nm. Below this grain size, the fundamental deformation mechanisms begin to change, and either a plateau or decrease in strength has been observed with further decreasing grain size [1].

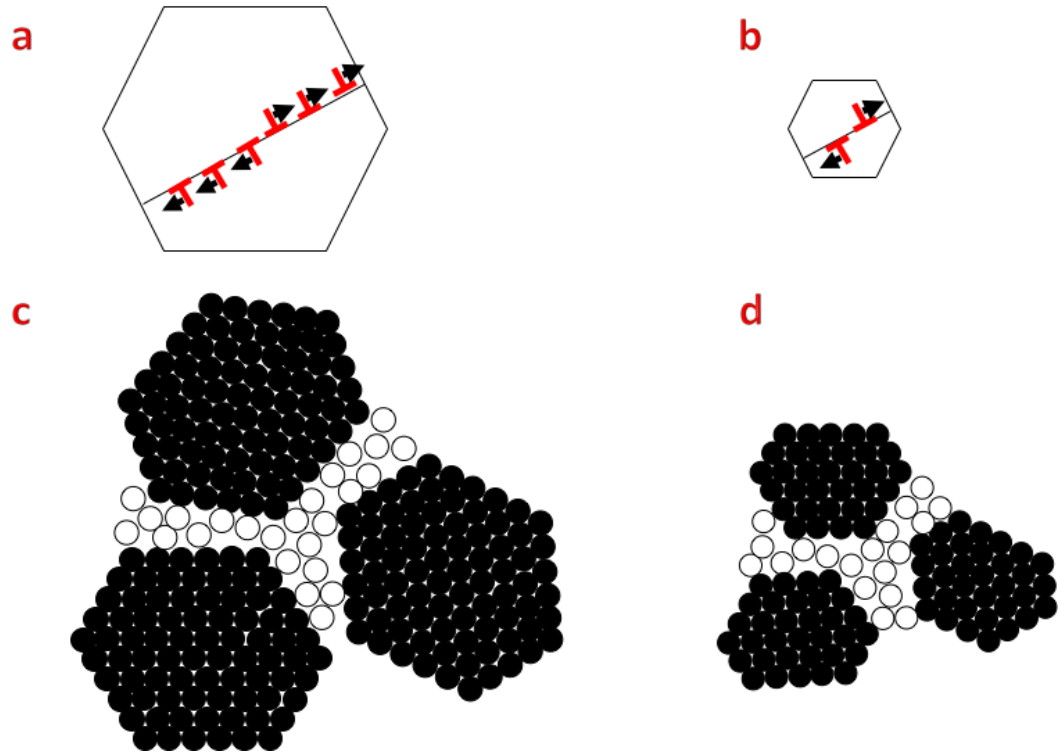

Figure 1.1: Comparison of microcrystalline and nanocrystalline materials. Comparison of dislocation pile-ups in (a) a microscale grain and (b) a nanoscale grain which can no longer fit multiple dislocations. Comparison of number of atoms in the grains and grain boundaries for (c) microcrystalline materials and (d) nanocrystalline materials. Figures not drawn to scale.

The exact mechanisms of plastic deformation which replace dislocation pile-ups in nanocrystalline metals are still debated, but contenders are grain boundary sliding, rotation, migration, and dislocation absorption and emission at grain boundaries [1]. More generally, there appear to be multiple deformation mechanisms which occur and can dominate deformation in materials with very small grain sizes. In some cases plasticity is dislocation-mediated and in others it is grain boundary-mediated. For example, Kumar et al. investigated the deformation of electrodeposited, fully dense, nanocrystalline Ni with a grain size of ~ 30 nm by (1) tensile testing in situ in a transmission electron microscope (TEM) (2) TEM characterization of samples post-deformation by compression and nanoindentation [5]. They found that deformation was dominated by dislocation-mediated plasticity. They observed that deformation

started with the emission of dislocations at grain boundaries, followed by the creation and growth of voids at grain boundaries and triple junctions due to intergranular slip and grain boundary sliding. These voids then acted as nucleation sites for dimples which lead to fracture [5]. However, Shan et al. found contrasting results with in-situ TEM studies of nanocrystalline Ni with a grain size of 10 nm [6]. They found that deformation was dominated by grain boundary mediated processes, particularly grain rotation leading to the formation of grain agglomerates. Nevertheless Shan et al. also found trapped lattice dislocations in grains post-deformation, indicating that there is still some dislocation-mediated deoformation [6].

Besides experimental work, a number of molecular dynamics (MD) simulation studies have helped to elucidate the mechanical properties and deformation of nanocrystaline materials. These simulations generally show that for materials with grains larger than 10-12 nm, plasticity occurs my a mixture of inter- and intra-grain deformation mechanisms, where the intra-grain deformation mechanisms take the form of dislocations propagating through grains and being nucleated/annihlated at grain boundaries. Below a critical grain size, inter-grain deformation mechanisms become dominant [7]. Futhermore, in materials with grain sizes less than 30 nm, only partial dislocations are observed [7]. However, there are many limitations to MD simulations. For one, they must be done using high strain rates (10^7 - 10^9/s). Additionally, they are sensitive to the chosen grain boundary structure, which could dramatically vary with the addition of impurities commonly introduced by experimental fabrication methods [8]. In a review of MD simulation work on nanocrystalline materials, Derlet et al. concluded the only meaningful information which can be drawn from these simulations is determining the atomic processes taking place during deformation [7].

1.3 Nanocrystalline Ni

Nanocrystalline Ni is one of the most widely studied nanocrystalline metals. In a survey of literature data for the yield stress and hardness of Ni across a large range of grain sizes (d = 10 nm – 460 μm), Cordero et al. found that for the aggregated data the Hall-Petch slope was k = 7.3 GPanm$^{1/2}$ with an intercept σ_0 = 0.08 GPa [4]. For Ni, $Gb^{1/2}$ = 38 GPAmn$^{1/2}$, so $k/Gb^{1/2}$ = 0.2 as with most FCC metals. We have aggregated hardness data specifically for nanocrystalline Ni (d = 3 - 660 nm). The data are shown on a Hall-Petch plot in Figure 1.2. In order to compare out results to Cordero et al., we can multiply the k and σ_0 values Cordero et al. found by a Tabor factor of 3. Doing this we get k_H = 22 GPanm$^{1/2}$ and σ_{0H} = 0.24

GPa. From our aggregated data we found $k_H = 16$ GPanm$^{1/2}$ and $\sigma_{0H} = 1.7$ GPa by fitting the data for which $d > 20$ nm. For grain sizes below 20 nm, one can see the start of a plateau in hardness with respect to $d^{-1/2}$. The discrepancy in values could come from the testing method and the assumption that Tabor's relationship is valid ($H = 3\sigma_y$). Other studies which specifically looked at hardness values for nanocrystalline Ni have found Hall-Petch slopes $k_H = 15$ GPanm$^{1/2}$ closer to what we found [9]. Table 1.1 shows values for k_H and σ_{0H} from individual datasets. There is significant variation in values, indicating that these values are very sensitive to sample type and experimental methods. In the next chapter we will discuss some of the factors other than grain size which can impact the hardness of nanocrystalline metals.

Figure 1.2 shows the same aggregated data as Figure 1.1 but plotted on a log-log plot. The fitted line has a slope of -0.31, while we would expect a slope of -1/2 if the Hall-Petch relationship is strictly followed. Cordero et al. found similar results, specifically an exponent of -0.39 for Ni, as well as exponents ranging from -0.03 for Hf to -0.95 for W [4]. There is still more work to be done in determining the generality of the exponent in the Hall-Petch relationship.

k_H	σ_{0H}	Reference
22	0.24	[4]
22.5	0.551	[11]
17.2	2.33	[12]
21.2	1.76	[13]
16.6	1.66	[14]
22.6	1.59	[15]
16.0	2.09	[16]
19.3	1.82	[17]
14.8	3.77	[18]
17.5	1.56	[19]
17.7	0.868	[23]
16	1.7	Aggregated Data

Table 1.1: Values for k_H and σ_{0H} from individual datasets.

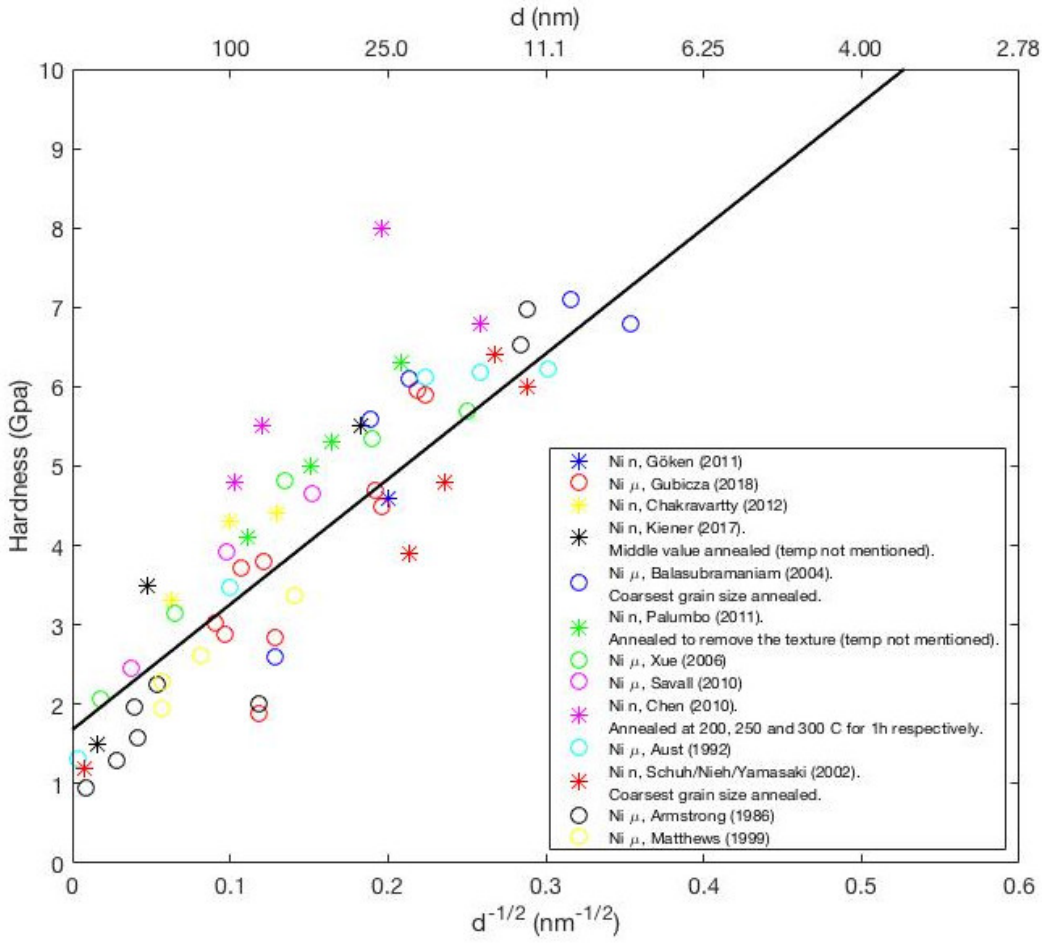

Figure 1.2: Hall-Petch plot for nanocrystalline Ni. The fitted line is $H = 1.7 + 16d^{-1/2}$. Data are from [10–22].

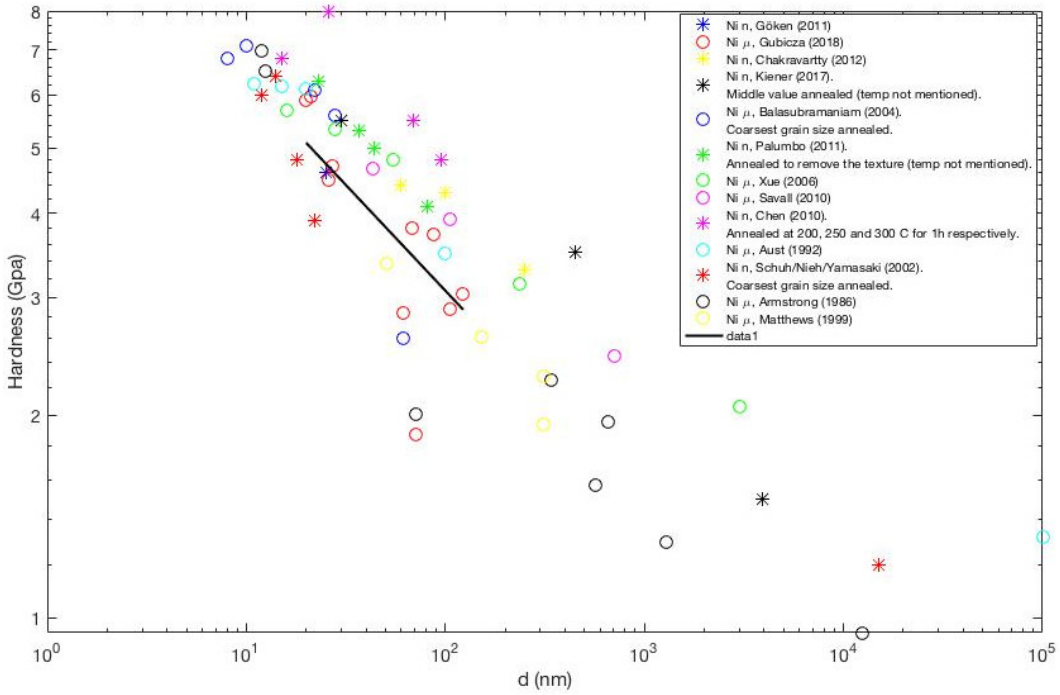

Figure 1.3: Hardness versus grain size for Ni on a log-log plot. Data are from [10–22].

Chapter 2

FACTORS OTHER THAN GRAIN SIZE CONTROLLING THE HARDNESS OF NANOCRYSTALLINE NI: ADDITIVES, ANNEALING, AND TEXTURE

In the last chapter we discussed the dependence of the hardness of materials, both coarse-grained and nanocrystalline, on grain-size. In this chapter we review other factors which affect the hardness of nanocrystalline materials and can lead to deviations from the Hall-Petch relation. These factors include alloying or solid-solution addition of other elements, annealing, and texture.

2.1 Additives to Nanocrystalline Ni

There are several elements which are commonly used as additives for nanocrystalline Ni. These additives include but are not limited to Co [24], Fe, Cu [15], and P [25, 26]. However, by far the most common additive for nanocrystalline Ni is W [27–31].

Much of the interest in using W as an additive comes from the discovery that W addition can be used to tune the grain size of nanocrystalline Ni and to achieve smaller grain sizes (~2 nm) compared to what is possible with pure metals like Ni (~20 nm) [32]. In a single-component system like pure Ni, there is a positive grain boundary energy, so the system can lower its free energy by reducing the volume of grain boundaries or equivalently by increasing the grain size. Thus, it is non-trivial to fabricate nanocrystalline materials as they are inherently unstable with respect to grain growth. However, in a two-component system, the free-energy of the system can be lowered by segregating one component to the grain boundaries. If the energy reduction for segregation is high enough, the grain boundary energy will equal zero at an equilibrium grain size, leaving no driving force for grain growth and allowing nanocrystalline materials to be accessed in an equilibrium state. Detor and Schuh were able to fabricate Ni-W samples with compositions ranging from 1.2 to 26.5 at% W by electrodeposition [32]. This ability to tune the W content also allowed them to tune the grain sizes between 2 and 140 nm, with higher W content producing smaller grains.

It should be noted here that Detor and Schuh only observed FCC Ni-rich solid

solutions, even for W contents of 26.5 at%, while the equilibrium phase diagram for Ni-W indicates a solubility limit of 12 at%. The phase diagram for Ni-W is shown in Figure 2.5 [35]. While this might seem to indicate that the samples with high W content are not at equilibrium and unstable, this is simply another result of grain boundary segregation. Atom probe tomography experiments have shown that for Ni-W with d = 16 nm and d = 28 nm, the grain-boundary (grain-interior) compositions were 27 (19) and 23 (14) at.% W, respectively [33]. Thus, the compositions of the grain interiors are much closer to the solubility limit expected from the phase diagram. Furthermore, while W content is intimately linked to grain size, the excess W content in the grain boundaries compared to the grain interiors is relatively independent of grain size. For Ni-W with grain sizes ranging from d = 3 nm to d = 28 nm, the excess W-content in the grain boundaries is relatively constant at 4-8 at.% W [33, 34]. Similar tuning of grain sizes has been done with P content in Ni. However, P has much lower solubility in Ni than W, which limits its tuning ability to very fine grain sizes. Liu and Kirchheim were able to tune between 2 and 9 nm with compositions of 3 - 13 at.% P [26].

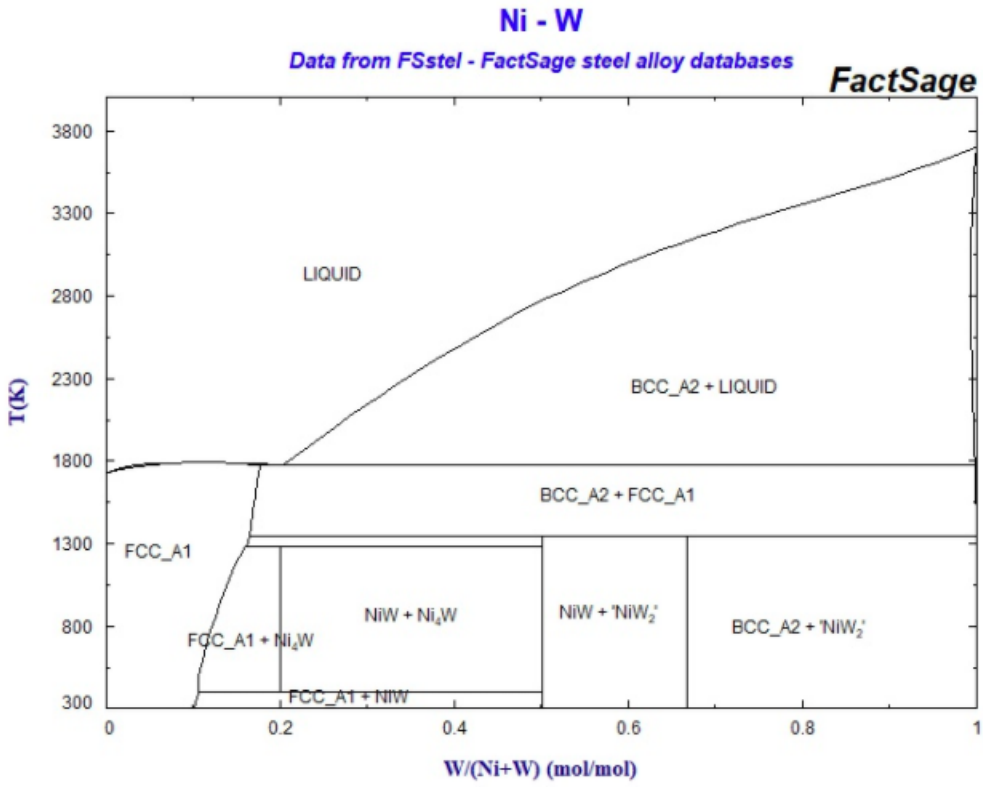

Figure 2.1: Phase diagram for Ni-W system. Reproduced from [35].

While the purpose of using W as an additive may be to allow for finer control

of grain size, W addition has other affects on the mechanical properties of nanocrystalline Ni. Figure 2.4 shows a Hall-Petch plot for both nanocrystalline Ni and Ni-W. From Figure 2.4 it is apparent that Ni-W solid solutions typically have higher hardness compared to Ni. The most obvious explanation for this is solid solution hardening; the large W atoms in the Ni lattice create a stress field which impedes dislocation motion. However, Schuh et al. have pointed out that the solid solution hardening affect of adding W to Ni is expected to increase the hardness by about 40 MPa, which is very small compared to the hardness of pure nancrystalline Ni at around 7 GPa [30]. While the model Schuh et al. used to obtain this estimate for the increase in hardness did not explicitly account for dislocation emission from grain boundaries or W segregation to the grain boundaries, it should give a reasonable order of magnitude estimate [30]. Initially, Schuh et al. attributed the increased hardness of nanocrystalline Ni-W to the fact that W addition produces finer grain sizes [30]. However, the data in Figure 2.4 suggest that Ni-W has a higher hardness than Ni even at the same grain size. Furthermore, this increase in magnitude appears to be on the order of GPa's rather than tens of MPa's. In a more recent paper Schuh and colleagues demonstrate a technique to fabricate Ni-W solid solution with different concentrations of W but holding the grain size constant at $d = 20$ nm [36]. They found that W addition does indeed increase hardness independently of the refinement of grain size. This is in agreement with data we have collected from the literature shown in Figure 2.4. Their explanation was that in addition to traditional solid solution hardening, the addition of solutes to nanocrystalline materials affects the global properties, including shear modulus and burgers vector, without affecting the primary deformation mechanism [36]. Other possible experimental factors contributing to this increase in hardness could be that nanocrystalline Ni-W samples might tend to be textured differently or have differently shaped grains than nanocrystalline Ni samples.

Given that W composition is generally intimately linked to grain size in electrodeposited nanocrystalline Ni-W and that hardness is dependent on grain size, it is difficult to determine if hardness is affected by W addition from a survey of the literature. However, by sputtering Ni-W, Rupert et al. were able to acheive Ni-W samples with a composition range of 0-20 at.% W all for the same grain size $d = 20$ nm [36]. Their data is shown in Figure 2.2 and Figure 2.3. Both hardness and Young's modulus increase with increasing W content indepent of the effect on grain size.

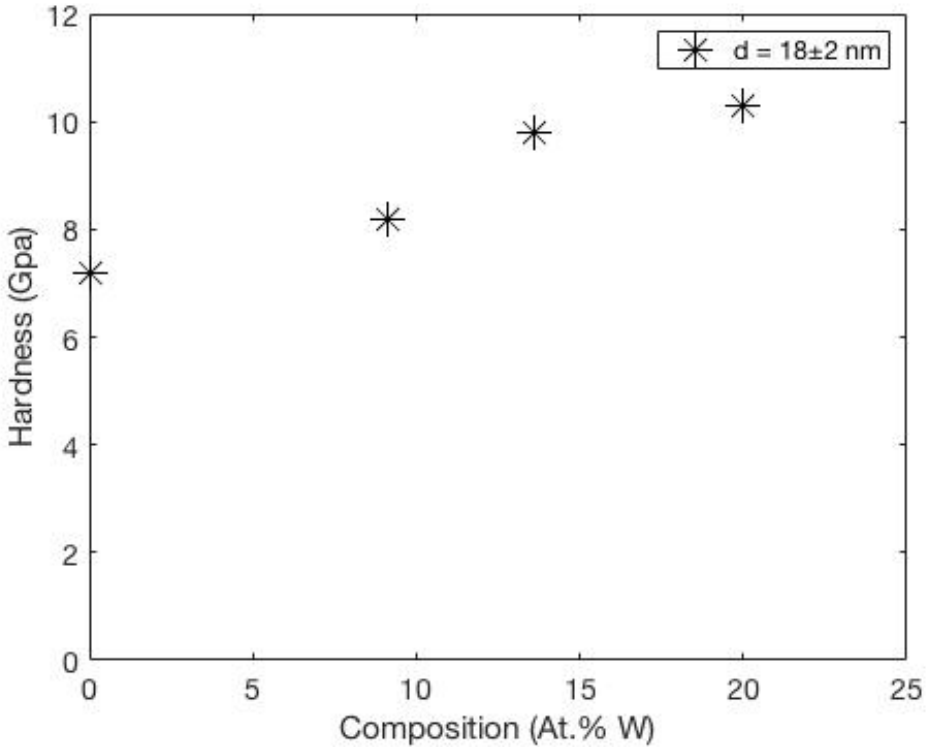

Figure 2.2: Hardness for Ni-W samples for different W contents. Data are from [36].

Another change in mechanical properties caused by W addition to nanocrystalline Ni is the shift of the grain size at which the Hall-Petch breakdown begins to occur to smaller grain sizes. Although it can be harder to see the Hall Petch breakdown with pure nanocrystalline Ni due to the instability of very fine Ni grains, the aggregated data in Figure 2.4 suggest that for Ni the Hall-Petch relation breaks down at a grain size of ~13-25 nm while for nanocrystalline Ni-W this break down occurs at smaller grain sizes, ~8-12 nm. This decrease in "inflection grain size" requires that W addition suppresses deformation at very fine grain sizes.

Although there is still significant debate surrounding the mechanisms for the breakdown of the Hall-Petch effect (see Chapter 1), Schuh & Nieh have provided a model for how W addition could suppress diffusive deformation mechanisms [23]. For a solid solution under steady state conditions the solution components must redistribute during deformation to maintain chemical homogeneity. Therefore, the deformation is controlled by the diffusivities of both components. Following Schuh & Nieh, assuming a steady-state Coble-creep deformation mechanism, the

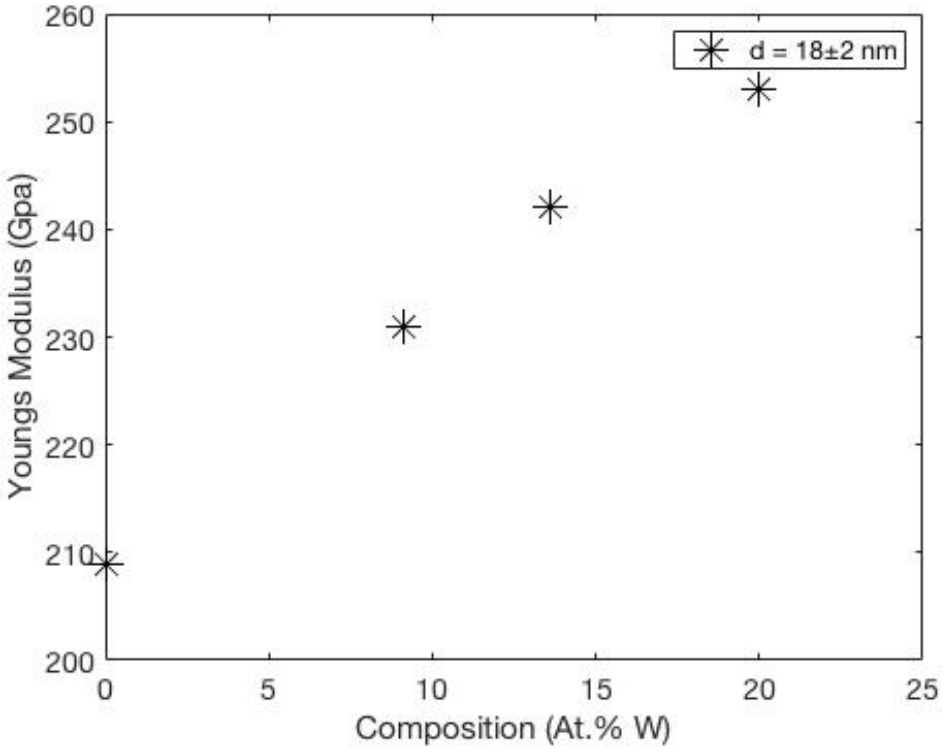

Figure 2.3: Hardness for Ni-W samples for different W contents. Data are from [36].

inflection grain size for a concentration of substitutional element (in this case W) can be estimated as:

$$\frac{d_{Ni-W}}{d_{Ni}} = \left[\frac{D_W}{D_{Ni}}(1-c)+c\right]^{2/7} \tag{2.1}$$

where d is the inflection grain size and D is the grain boundary diffusivity. For a deformation mechanism where diffusion occurs predominantly within the grains like Nabarro-Herring creep, the exponent would be 2/5 [23]. There are no reported values for D_W and D_{Ni}, but W is much larger than Ni with an atomic radius of 210 pm compared to 163 pm for Ni. Consequently, at room temperature, the diffusivity of W in Ni is smaller than the self-diffusivity of Ni by a factor of 10^{-15}. Therefore, Schuh & Nieh assume

$$\frac{D_W}{D_{Ni}} \approx 0 \rightarrow \frac{d_{Ni-W}}{d_{Ni}} \approx c^{2/7} \tag{2.2}$$

Thus, for a W concentration of $c = 0.26$ we would expect $\frac{d_{Ni-W}}{d_{Ni}} = 0.68$. For $c = 0.12$ we would expect $\frac{d_{Ni-W}}{d_{Ni}} = 0.55$. If, based on the data in Figure 2.4, we take $d_{Ni-W} = 10$ nm and $d_{Ni} = 18$ nm, we get $\frac{d_{Ni-W}}{d_{Ni}} = 0.56$, in good agreement with this estimate.

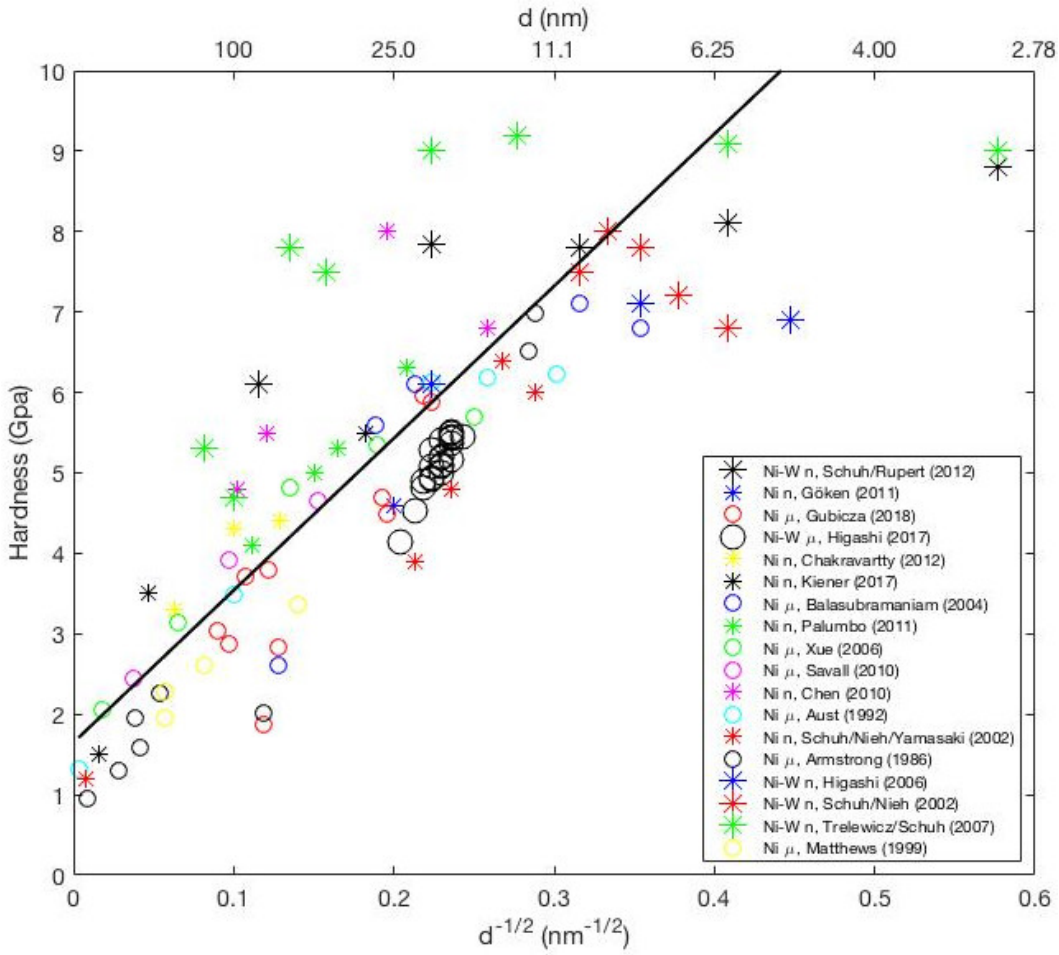

Figure 2.4: Hall-Petch plot for Ni and Ni-W. The fitted line ($H = 18.9x + 1.65$) represents the Hall-Petch relation. Data are from [10–20, 22, 27–31].

2.2 Annealing

It has been reported by many studies that as-prepared nanocrystalline metals have nonequilibrium grain boundaries which contain dislocations, excess free volume, and misfit regoins [37–39]. It has also been shown that annealing relaxes these nonequilibrium grain boundaries, which become more ordered and are eliminated of excess defects [37, 40]. This process is called grain boundary relaxation. Figure 2.5 shows data collected from the literature for both unannealed and annealed nanocrystalline Ni-W. It is clear that annealing increases hardness for Ni-W. The mechanism for this increase in hardness with annealing is generally thought to be grain boundary relaxation.

Ni-W is thermally stable below ~500°C. Above this temperature, grain growth begins to occur, but ultrafine grain structures are kept up to a temperature of ~900°C

[41]. All of the annealed data included in Figure 2.5 is for an annealing temperature well below 500°C, so it can be assumed that the observed increases in hardness are not related to changes in grain size. Detor & Schuh have shown that the heat released during low temperature annealing of Ni-W scales with grain boundary area which in turn increases with decreasing grain sizes [41]. This observation supports the explanation of grain boundary relaxation. Note that in Figure 2.5, there is also an apparent increase in the hardening due to annealing with decreasing grain size, which further supports this explanation.

Kinetic studies of hardening of Ni-W due to grain boundary relaxation have shown that hardness increases approximately linearly with annealing time until a maximum hardness is achieved [27]. This maximum hardness depends on annealing temperature, with higher temperatures allowing more pronounced as well as faster hardening [27]. An analysis of the rate of relaxation hardness at different temperatures for Ni-W and the calculated activation energies led Rupert et al. to conclude that diffusion through triple junctions was the most likely mechanism to control the grain boundary relaxation kinetics. Rupert et al. proposed that the apparent dependence on maximum achievable hardness on temperature is caused by there being many different relaxation mechanisms occurring, some of which are only accessible at higher temperatures [27].

Once the grain sizes of nanocrystalline metals are reduced to ~1-2 nm, these materials begin to reach the limit of amorphous metals. In Figure 2.5 one can see that the increase in hardness due to annealing increases with decreasing grain size up until a grain size of ~6 nm. At ~3 nm the increase in hardness due to annealing is less dramatic. Rupert et al. have also observed that there is increased shear localization during deformation of Ni-W with $d = 3$ nm after annealing [27]. A similar phenomena has been observed in metallic glasses whereby annealing or increasing the order in glasses leads to more localized plastic flow [27]. This suggests that nanocrystalline metals with $d = 3$ nm are entering the metallic glass regime.

2.3 Texture

Texture is another factor which affects the hardness of nanocrystalline materials and can make samples appear to deviate from the Hall-Petch relation. There are five possible preferred orientations which have been observed in electrodeposited nanocrystalline Ni: (100), (110), (210), and (211), as well as randomly distributed

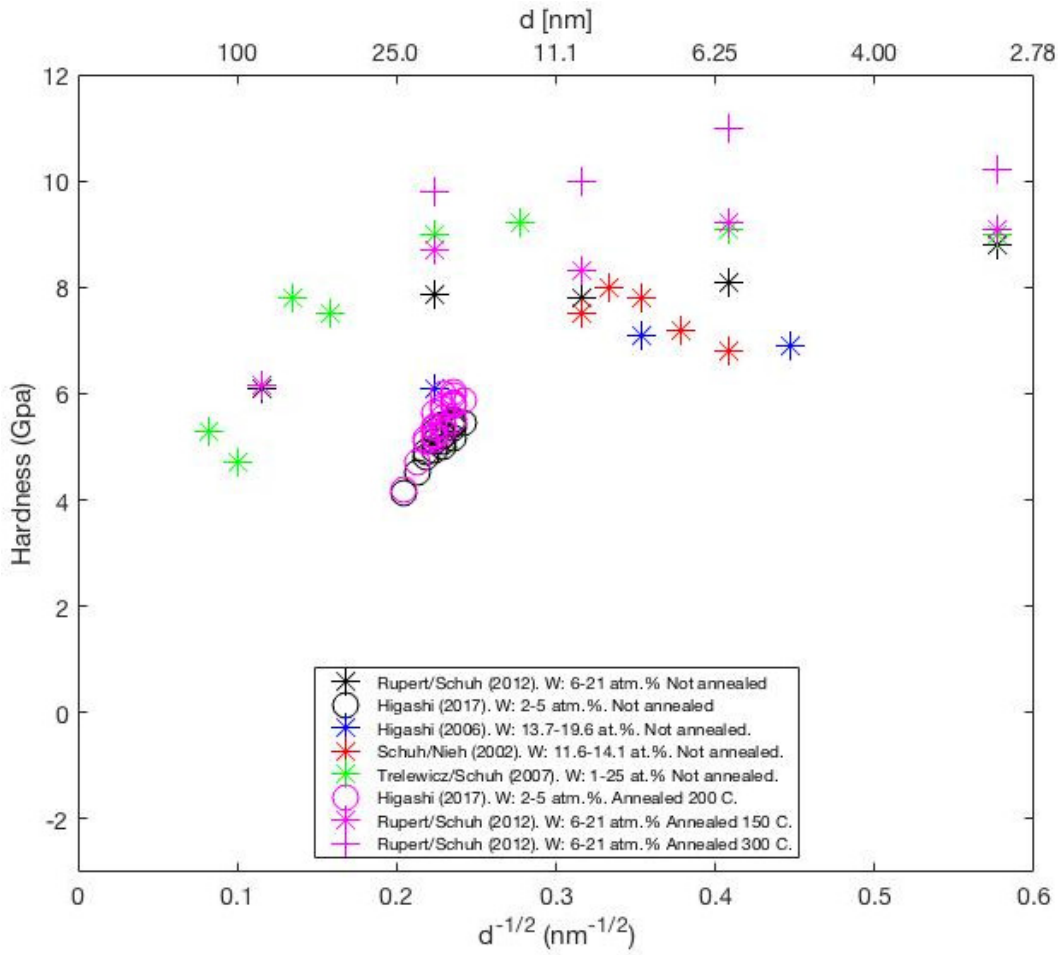

Figure 2.5: Hall-Petch plot for annealed and unannealed nanocrystalline Ni-W. Data from [23, 27–29, 31].

grain orientation [17, 42]. The texture is dependent on the electrodeposition conditions used. For example, higher current densities tend to produce more random texture and the ratio of time-on to time-off during pulsed plating can be used to select for specific textures [17, 30].

Furthermore, the grain size itself can be correlated with a specific texture. Godon et al. found that the texture of their electrodeposited nanocrystalline Ni samples had three different grain size regimes, each with a different texture and a different Hall-Petch slope [17]. The first regime ($d = 278 - 816$ nm) corresponded to a (100) texture, the second regime ($d = 51 - 278$ nm) corresponded to a (110) texture, and the last regime ($d = 33 - 51$ nm) corresponded to a random orientation of grains. The regime with (100) texture had the steepest Hall-Petch slope, while the regime with (110) had the least steep slope. The randomly texture regime had

an intermediate Hall-Petch slope similar to what has been found for polycrystalline Ni. Godon et al. attributed this variation in the Hall-Petch slope to competition between different physical mechanisms occurring near grain boundaries which are affected by grain orientation and grain boundary type [17].

2.4 Case Studies for Specific Grain Sizes

We now focus on two specific grain sizes in order to more fully demonstrate the combined effects of these factors above and below the Hall-Petch breakdown.

Case Study for $d = 75$ nm

Ni and Ni-W specimens with a grain size of 75 nm are well above the breakdown of Hall-Petch but still considered nanocrystalline and have a significant volume fraction of grain boundaries. Assuming spherical or cubic grains and a grain boundary thickness of 1 nm, we estimate the volume fraction of grain boundaries to be 4%. Most of the hardness data for Ni at this grain size is for pure Ni, given that it is fairly easy to fabricate pure nanocrystalline Ni at $d = 75$ nm compared to at smaller grain sizes ($d < 20$ nm). Of the literature data we have collected for pure Ni at this grain size the average hardness is $H = 3.5 \pm 1.5$ GPa. There are also a few data points available for Ni with low additions of W (~6 at.%) at this grain size, with average hardness $H = 5.4 \pm 1$ GPa. Thus, W addition appears to increase hardness. Annealing Ni-W at this grain size, by contrast, has very little affect. Figure 2.6. shows The hardness of Ni-W after annealing at different temperatures. There is only a 50 MPa difference in hardness between unannealed and annealed samples.

Case Study for $d = 6$ nm

Almost all Ni samples at $d = 6$ nm grain size are a Ni-W solid solution due to the great difficulty of achieving stable pure Ni samples at this grain size. In our review of the literature, the smallest reported grain size for pure Ni we found was $d = 8$ nm [14]. The reported hardness of this sample was 6.8 GPa [14]. Of the literature we collected for Ni and Ni-W with grain sizes $d = 5 - 8$ nm, the average hardness was 7.4 ± 0.76 GPa. Both of these values are significantly above the hardness values we found for $d = 75$ nm, but are not quite as high as the peak hardness for nanocrystalline Ni-W at $H = 8 - 9$ GPa. For both Ni and Ni-W, a grain size of 6 nm is below the Hall-Petch breakdown. Trelewicz and Schuh have even suggested that Ni-W samples with $d = 6$ nm can be thought of as amorphous-matrix composites with 60% 6 nm crystal reinforcements [31]. The increased disorder in

materials at this grain size causes annealing to a have a greater impact on hardness (Figure 2.6).

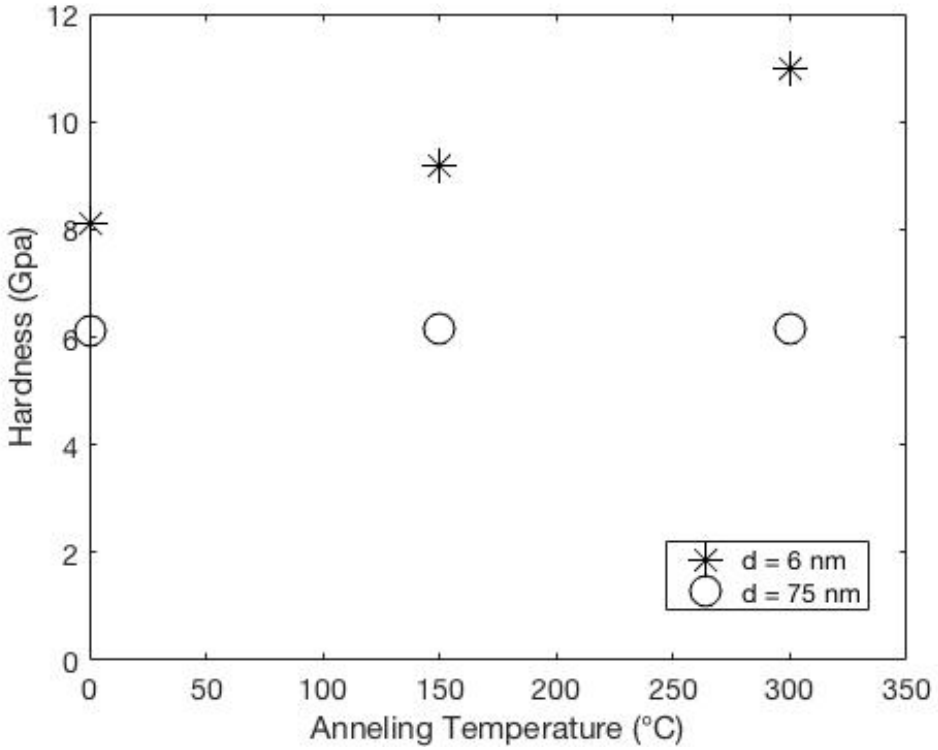

Figure 2.6: Hardness vs. annealing temperature for nanocrystalline Ni-W. Data from [27].

Chapter 3

FABRICATION, SEM CHARACTERIZATION, AND NANOINDENTATION OF NI FILMS

3.1 Fabrication of Ni Films

The method used for the fabrication of nanocrystalline Ni films in this work is an adaptation of the method described in Yee's paper for additive manufacturing of metal oxides [43]. First we prepared a photoresin by mixing 1 mL of 2.67M nickel nitrate hexahydrate solution with 1 mL of poly(ethylene glycol) diacrylate (PEGda) and 200μL of LAP solution (20 mg of lithium phenyl02,4,6-trimethylbenzoylphosphinate in 1 mL of water). The ratio of nickel nitrate hexahydrate solution to PEGda was varied for different samples and its effect will be discussed in a later section. We then sandwiched the resin between 2 glass slides (using additional glass slides as spacers) and cured the resin with 405 nm light. The time for which the resin was cured varied, but was typically 30 s – 2 min on each side. The resulting polymer films were approximately 1-2 mm in thickness and weighed approximately 0.5 – 2 g.

The polymer films were then calcinated with compressed air at 500°C at a pressure of 14 Torr. In order to reach 500°C, the heating rate was 0.5°C/min followed by a cooling rate of 2°C/min. This resulted in NiO films. The film mass after calcination was greatly reduced, 50 – 150 mg. Finally, to achieve Ni films, the NiO films were reduced in forming gas (95% N_2, 5% H_2) at a pressure of 14 Torr and a temperature of 700°C for 6 hours.

Note that while in this work we focus on films made by this process, the same general method can be used to make complex 3D geometries at the nanoscale by patterning the resin using two-photon lithography instead of curing with a light [43].

3.2 Resulting Microstructure

SEM images of the nanocrystalline Ni films are shown in Figure 3.1. The fabrication for Samples 1, 2, and 3 were identical with the exception of the ratio of nickel nitrate hexahydrate solution to PEGda used. Samples 1, 2, and 3 had ratios of nickel nitrate hexahydrate to PEGda of 40:60, 50:50, and 60:40, respectively. Sample 4 had a ratio of 50:50, but differed from Sample 2 in that the resin was only

cured for 30 seconds on each side instead of 1 minute.

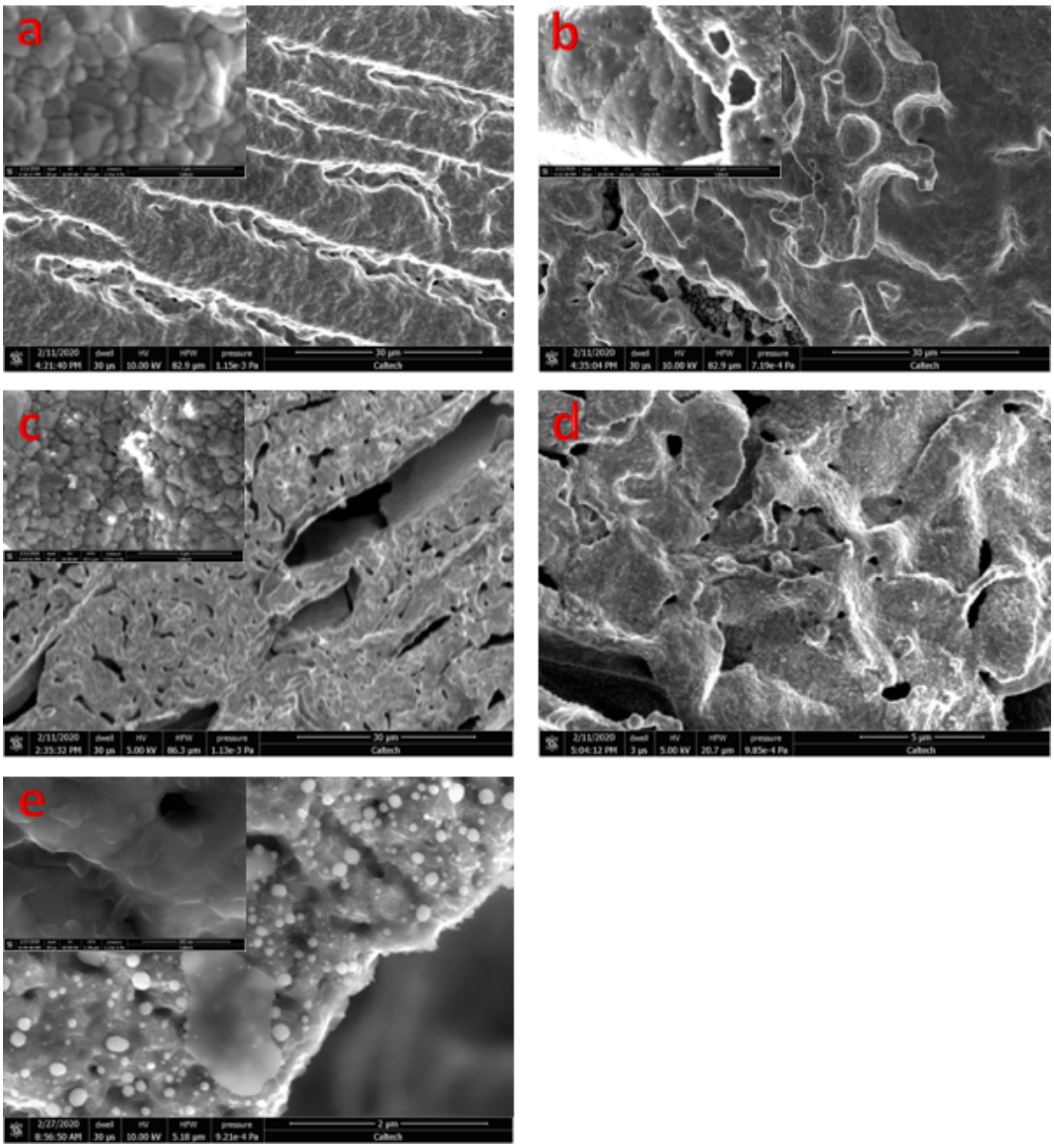

Figure 3.1: SEM images of nanocrystalline Ni films. (a) and (b) two different regions of Sample 1, (c) Sample 2, (d) Sample 3, and (e) Sample 4.

There are several significant features of the microstructure of the films. All of the samples have a number of pores on the surface. While we are unsure of the exact porosity of the films, based on these images we would not be surprised if they were as much as 50% porous. A number of cracks are also visible in each of the films. Furthermore, there is evidence of impurities in the SEM images. Looking at the images of Sample 4, for example, the bright white spheres on top of the Ni grains are likely some contaminant from the fabrication process. One last aspect

of the microstructure that should be noted, is that there is significant variation in microstructure across individual samples. Consider Sample 1, for example. Some regions of the sample have regular ridges while others have more irregular folding patterns.

SEM images were used to estimate the average grain sizes of Samples 1, 2, and 3, and all three of these films were found to have grain diameters in the range of hundreds of nanometers. Histograms showing counts for the number of grains of each diameter are shown in Figure 3.2 for two different regions of each sample. The mean grain size is 445 ± 226 nm, 298 ± 104 nm and 199 ± 53 nm for Samples 1, 2, and 3, respectively. The grain size decreases with increasing ratio of nickel hexahydrate solution to PEGda. This observation is unsurprising; higher Ni loading would create a higher density of nucleation sites for the Ni grains and lead to the growth of smaller grains.

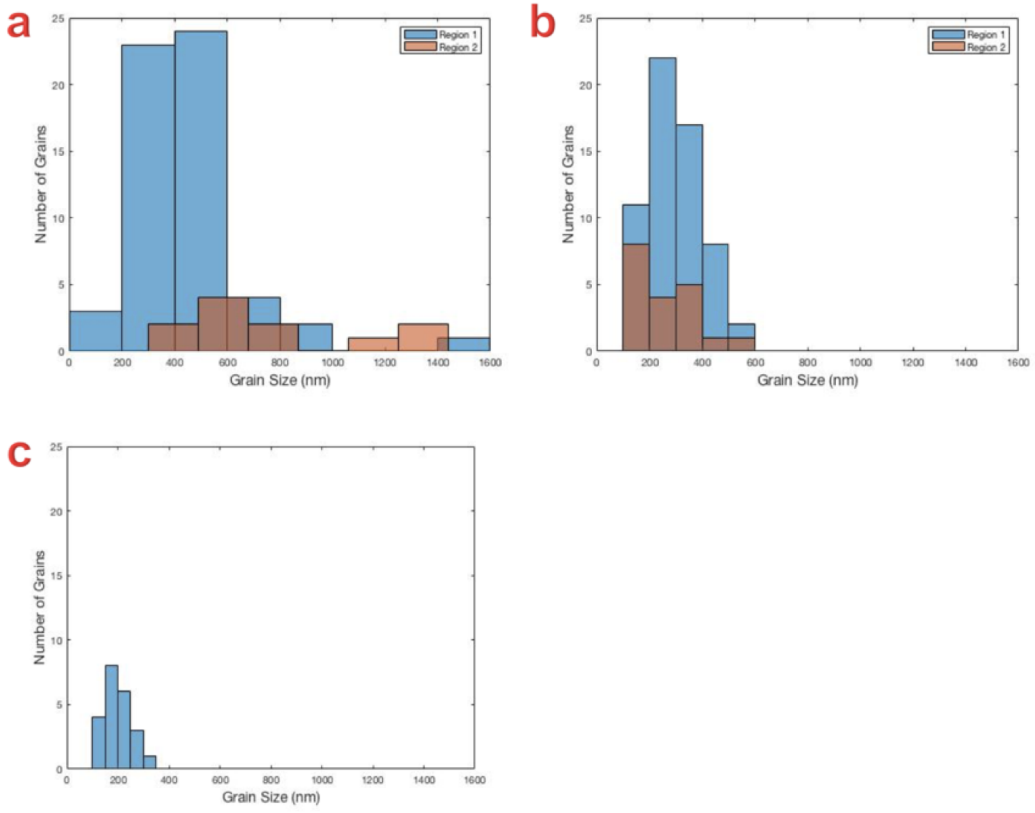

Figure 3.2: Counts of grains of different diameter ranges for Samples (a) 1, (b) 2, and (c) 3.

3.3 Nanoindentation

Nanoindentation was performed on the Ni films using a G200 Nano Indenter with a Berkovich tip. The indents were done to a depth of 5 – 10 μm. The thickness of the films were at least 350 μm, so there should be no effect of the thickness on the measured hardness. A representative force vs. displacement curve is shown in Figure 3.3.

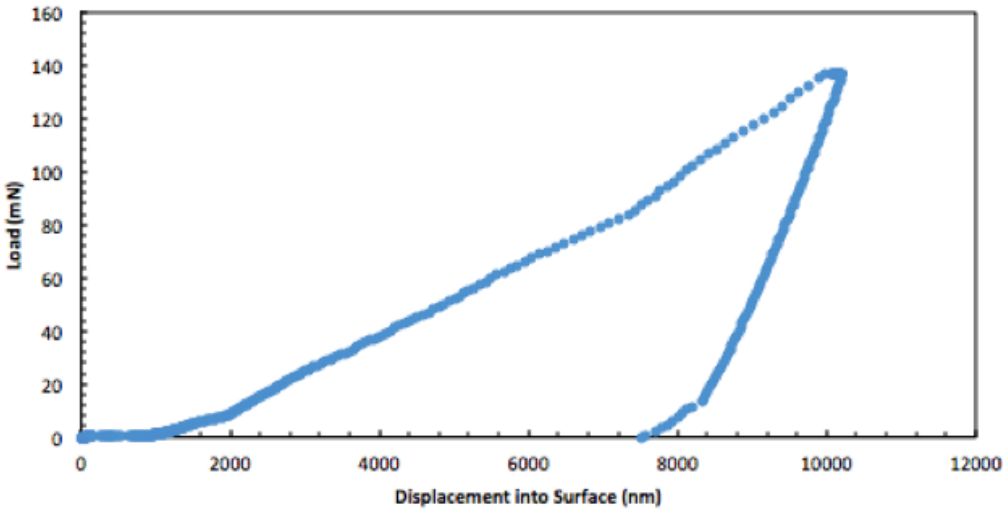

Figure 3.3: Force vs. displacement during nanoindentation of Sample 2.

The reduced modulus and hardness of the samples were calculated following the method of Oliver and Pharr [44]. The reduced modulus is calculated as

$$E_r = \frac{\sqrt{\pi}}{2}\frac{S}{\sqrt{A}} \tag{3.1}$$

where A is the contact area and S is the measured stiffness. The contact area as a function of contact depth for the Berkovich tip used was found experimentally to be $A(h) = 24.5h_c^2 + 688h_c$ prior to analysis. The contact depth at peak load was determined using the equation

$$h_c = h_{max} - h_s \tag{3.2}$$

where h_{max} is experimentally measured and h_s is the displacement of the surface of the contact perimeter

$$h_s = \epsilon\frac{P_{max}}{S} \tag{3.3}$$

For Berkovich indenters, $\epsilon = 0.75$. The stiffness S was calculated from the unloading data. The unloading data was fit by a simple power law relation:

$$P = A\left(h - h_f\right)^m \tag{3.4}$$

The stiffness S was found by analytically differentiating this expression and evaluating the derivative at the peak load and displacement. Hardness was computed as

$$H = \frac{P_{max}}{A} \tag{3.5}$$

Performing these calculations on our nanoindentation data for Sample 2, we found $H = 0.056$ GPa and $E_r = 1.76$ GPa.

Chapter 4

MODELING MODULUS AND HARDNESS OF NANOCRYSTALLINE NI AS A FUNCTION OF GRAIN SIZE AND POROSITY

As discussed in Chapter 3, we calculated that our fabricated nanocrystalline Ni films had a hardness of $H = 0.056$ GPa and a reduced modulus of $E_r = 1.76$ GPa. Based on the values from the literature presented in Chapters 1 and 2, we would expect the hardness and reduced modulus to be ~2.6 GPa and ~207 GPa, respectively. The measured values are two orders of magnitude lower than these values.

Historically, early investigations into the Young's modulus of nanocrystalline metals produced conflicting results. Some studies showed that the Young's modulus of nanocrystalline metals produced by inert gas condensation were reduced by over 50% compared to coarse-grained metals [45]. However, later studies confirmed that compacted nanocrystalline materials have modulus values near that of polycrystalline materials and that the low previously measured value for moduli were due to residual porosity in the samples [15]. Therefore, porosity might be a significant factor in why the values of hardness and modulus we measured are so low. In this chapter we examine how the modulus and hardness of nanocrystalline materials depends on porosity and grain size in order to determine whether these factors can account for these anomalously low values.

4.1 Models for Modulus Dependence on Grain Size and Porosity

We model the dependence of modulus on grain size following Giallonardo et al. [15]. We consider the contribution of three different structural components – grain interiors, grain boundaries, and triple junctions. The influence of each of these components can be estimated using a simple rule of mixtures:

$$E(d) = E_0 f_g(d) + E_{gb} f_{gb}(d) + E_{tj} f_{tj}(d) \tag{4.1}$$

where E_0 is the Young's modulus of the bulk polycrystalline material, E_{gb} is the Young's modulus of the grain boundaries, E_{tj} is the Young's modulus of the triple junctions, and $f_x(d)$ is the grain size-dependent volume fraction of each component.

If we assume a 3D tetrakaidekahedral crystal shape, the volume fractions are:

$$f_g(d) = 1 - f_{ic}(d) \tag{4.2}$$

$$f_{ic}(d) = 1 - \left(\frac{d-t}{d}\right)^3 \tag{4.3}$$

$$f_{tj}(d) = 1 - \frac{3t(d-t)^2}{d^3} \tag{4.4}$$

where $f_{ic}(d)$ is the intercrystallite volume fraction. We assume that the grain boundary thickness is $t = 1$ nm and that E_{gb} and E_{tj} are about 76% and 73% of E_0, respectively. These assumptions come from values Zhou et al. found by applying the same model to nanocrystalline Ni-3wt% P [25]. We apply this model to nanocrystalline Ni, which has a polycrystalline Young's modulus of $E_0 = 207$ GPa [15]. A plot for the expected variation in Young's modulus with changing grain size for nanocrystalline Ni is shown in Figure 4.1. Above a grain size of ~50 nm, the Young's modulus is practically at its conventional polycrystalline value, and there is little dependence of modulus on grain size. However, below ~20 nm the modulus decreases dramatically with decreasing grain size. This model using a simple rule of mixtures is in agreement with the results of MD simulations [46].

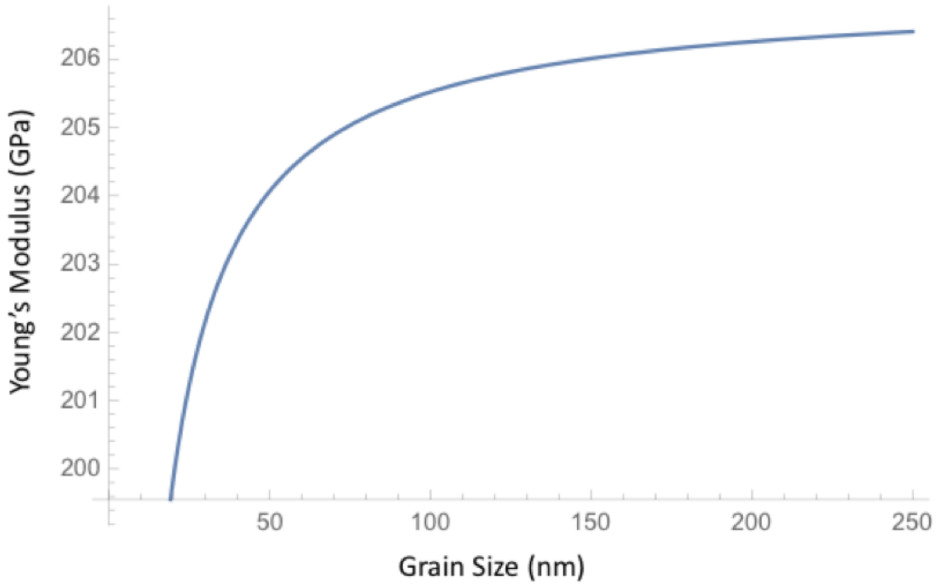

Figure 4.1: Predicted dependence of Young's modulus on grain size for fully-dense nanocrystalline Ni.

We model the dependence of modulus on porosity following Kristic et al [47]. Consider a nanocrystalline solid containing many non-interacting, uniformly distributed pores. For a nanocrystalline solid, it is highly unlikely that the surfaces of the pores are smooth. Thus, we assume that each of the pores contains annular flaws extending from its surface, as shown in Figure 4.2. The Young's modulus is then given by

$$E_p\left(V_p, \frac{S}{R}\right) = E_{d0}\left[1 + \frac{4V_p\,(1-v)}{\pi}\left(\left(1+\frac{S}{R}\right)^3 + \frac{9}{2\,(7-5v)\left(1+\frac{S}{R}\right)^2} + \frac{4-5v}{2\,(7-5v)}\right)\right]^{-1} \tag{4.5}$$

where E_{d0} is the Young's modulus of the fully dense nanocrystalline solid, V_p is the volume fraction of pores in the solid, v is the Poisson ratio, R is the pore radius, and S is the length of the annular flaw. The predicted Young's modulus of Ni versus porosity for different values of S/R is shown in Figure 4.2. The value of S/R has a dramatic effect on how the modulus decreases with increasing porosity; the modulus decreases much more rapidly for higher values of S/R.

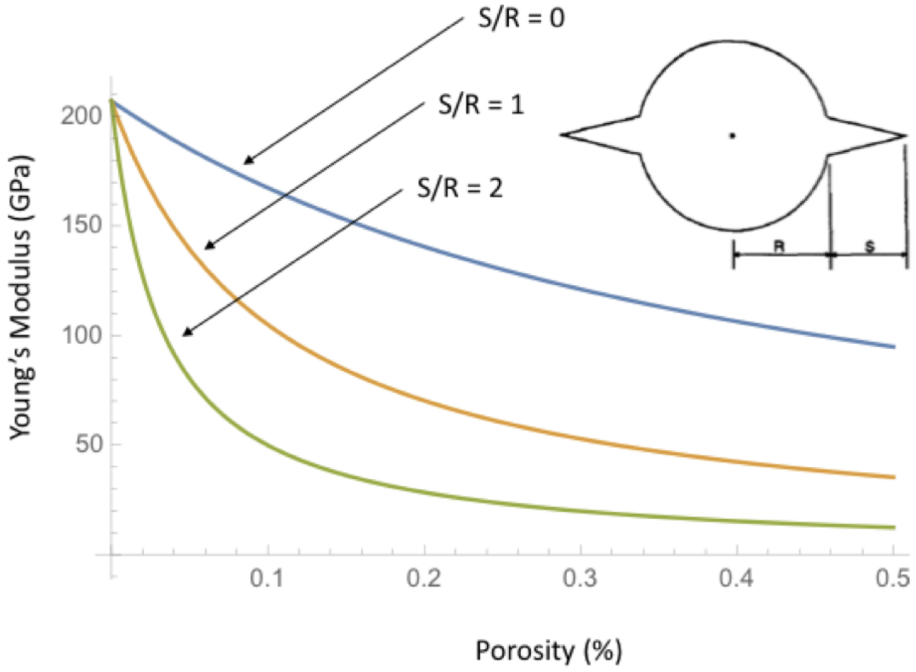

Figure 4.2: Predicted dependence of Young's modulus on porosity.

Combining these two models, we can plot the expected Young's modulus of a nanocrystalline, porous solid as in Figure 4.3. In Figure 4.3 there is also experimental data plotted for nanocrystalline Ni and Pd collected by Hurley et al.

[48] and Nieman et al. [45]. The experimental data shows good agreement with the model for $S/R = 1$.

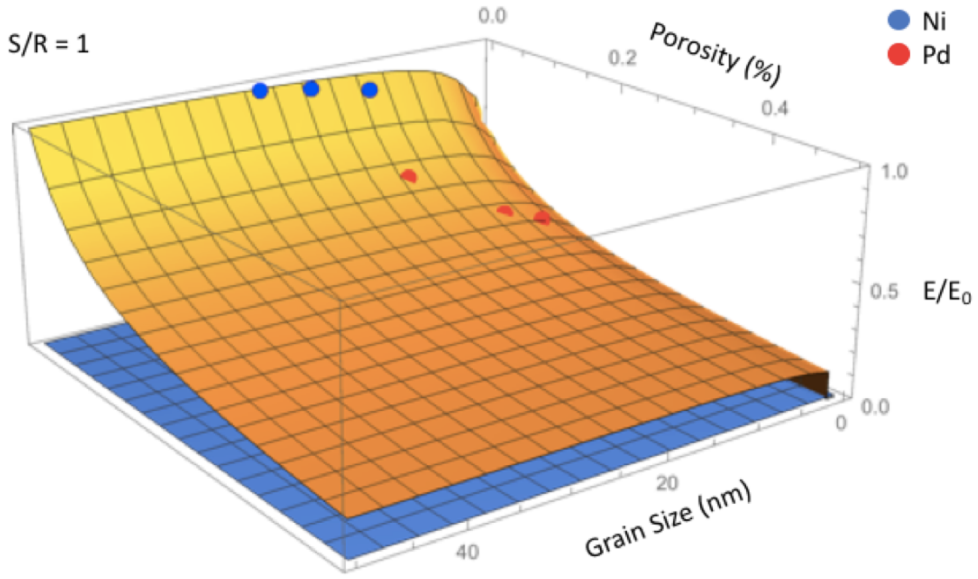

Figure 4.3: Combined model for dependence of Young's modulus on grain size and porosity.

Another factor which could affect the Young's modulus of nanocrystalline metals is texture. As with many FCC metals, the modulus of Ni varies greatly with orientation; in the (111) direction $E_{111} = 293$ GPa while $E_{100} = 130$ GPa [15]. Thus, one would expect nanocrystalline Ni samples which have a preferred (200) orientation to have a lower Young's modulus, and this is consistent with what has been observed by several authors. Fritz et al. found that by varying the current density used for electroplating nanocrystalline Ni, they could control the preferred orientation and by extension the Young's modulus between 165 GPa and 205 GPa [49]. Torrents et al. were able to control preferred orientation through annealing, and increased the Young's modulus of nanocrystalline Ni from 165 GPa to 240 GPa [50].

We can calculate the theoretical upper and lower bounds on the Young's modulus due to texture with the Voigt and Reuss bounds for statistically isotropic, polycrystalline, single-phase materials [15]. The bounds are determined by calculating the bulk and shear moduli:

$$K_V = K_R = \frac{c_{11} + 2c_{12}}{3} \tag{4.6}$$

$$G_V = \frac{c_{11} - c_{12} + 3c_{44}}{5} \tag{4.7}$$

$$G_R = \frac{5\,(c_{11} - c_{12})\,c_{44}}{4c_{44} + 3\,(c_{11} - c_{12})} \tag{4.8}$$

where K and G are the bulk and shear modulus, respectively, and the V and R subscripts represent the Voigt and Reuss bounds, respectively. The bounds on the Young's modulus are then determined by

$$\frac{1}{E} = \frac{1}{3G} + \frac{1}{9K} \tag{4.9}$$

For Ni, $c_{11} = 243$, $c_{12} = 149$, and $c_{44} = 119$ [51]. Performing this calculation, we find $E_V = 232$ GPa and $E_R = 194$ GPa. Experimentally, values outside these bounds have been observed. This indicates texture is important but certainly cannot account for variation in hardness values alone.

4.2 Models for Hardness and Yield Stress Correlation with Grain Size and Porosity

Besides elastic modulus, porosity has also been linked to anomalously low values of hardness in nanocrystalline materials. Ma et al. used a simple cluster-pore mixture model to describe the effect of porosity on hardness:

$$H_m = H_c\,(1 - p) + H_p p \tag{4.10}$$

where H_m is the measured hardness of samples, H_c is the hardness contribution of the clustered nanocrystalline grains, H_p is the hardness contribution of the pores, and p is the volume fraction of pores [24]. Since the pores do not contribute to the hardness ($H_p = 0$):

$$H_c = \frac{H_m}{1 - p} \tag{4.11}$$

Using this model, Ma et al. examined hardness measurements for porous electrodeposited nanocrystalline Co-Ni and Cu coatings which appeared to show a breakdown of the Hall-Petch effect at much larger grain sizes (~80 nm) than what is typically observed. They found that the calculated pore-free hardness actually did follow the Hall-Petch relation down to the smallest grain sizes measured [24].

Li presents a model which accounts for the grain size, impurity content, and porosity dependence of hardness [52]. Their model is based on the idea that at smaller grain sizes, the volume fraction of grain boundaries in a material is higher; thus, impurities which segregate to and are usually concentrated in the grain

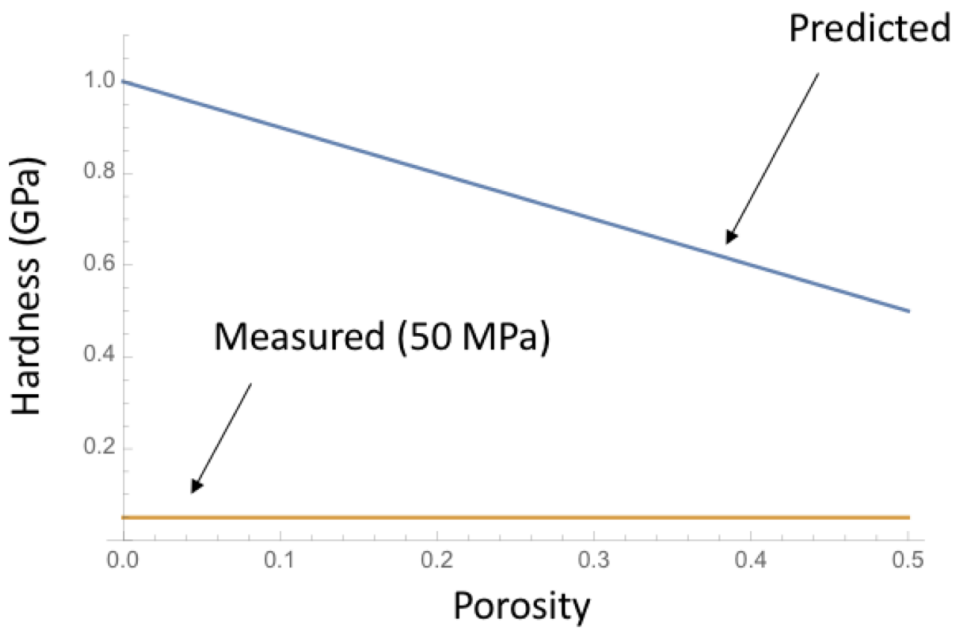

Figure 4.4: Predicted hardness as a function of porosity using the model developed by Ma et al [24] compared to experimental results discussed in Chapter 3.

boundaries become more dilute, and the grain boundaries effectively become more pure. It is thought that impurities in the grain boundaries stabilize ledges which serve as sources for dislocations. Therefore, there is a critical grain size between "impure" and "pure" grain boundaries, and for materials with grains smaller than this critical size, there is no longer an increase in stress required for deformation with decreasing grain size. The yield stress-grain size relationship based on this idea is

$$\sigma = \sigma_0 + A\sqrt{\frac{x}{\frac{d}{3}KN_0}} \tag{4.12}$$

where σ_0 is the yield stress for a single crystal, A is a constant, d is the grain size, K is the equilibrium constant for incorporation of impurities into the sample, N_0 is the saturation amount of impurity per unit area of grain boundaries, and $x = N/N_0$. Well above the critical grain size discussed above, the grain boundaries are saturated with impurities

$$x = x_m = \frac{KN}{1 + KN} \tag{4.13}$$

$$\sigma = \sigma_0 + A\sqrt{\frac{x}{\frac{d}{3}KN_0}} = \sigma_0 + A\sqrt{\frac{3KN_0}{d}} \tag{4.14}$$

which recovers the Hall-Petch relation [53]. However, as x or d approaches zero, the yield stress approaches

$$\sigma = \sigma_0 + A\sqrt{KN} \tag{4.15}$$

which provides an explanation for the Hall-Petch breakdown [52]. Porosity can be incorporated into this model by considering that if the grain boundary contains extra porosity, the internal stress distribution is altered and impurities are less segregated into the boundary. Therefore, we substitute

$$x \longrightarrow x - B\left(\phi - \phi_0\right) \tag{4.16}$$

$$\sigma = \sigma_0 + A\sqrt{\frac{x - B\left(\phi - \phi_0\right)}{\frac{d}{3}KN_0}} \tag{4.17}$$

where B is a constant, ϕ is the porosity, and ϕ_0 is the equilibrium porosity [52]. Figure 4.5 shows the expected yield strength based on this model for different values of $B\left(\phi - \phi_0\right)$.

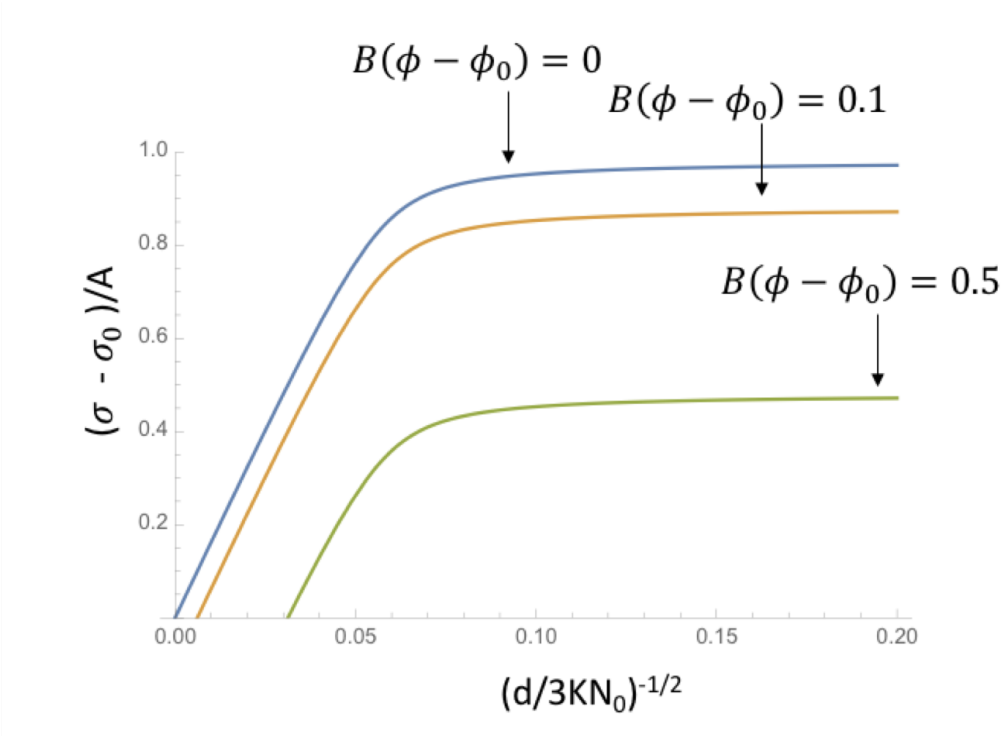

Figure 4.5: Grain size dependence of flow stress for different levels of porosity based on the model developed by Li [52].

Other authors such as Schiotz et al. have used atomic-scale simulations to study how porosity affects flow stress in nanocrystalline metals [54]. They found that the impact on the flow stress depends greatly on the type of pore, especially with higher levels of porosity. At 4-5% porosity, the type of pore had a small effect on the reduction in flow stress; elliptical, crack-like pores caused a 10-13% reduction in flow stress, missing grain boundary atoms caused a 5% reduction, and missing grains a 14% reduction. At 8-9% porosity there is a more noticeable difference. Missing grains cause a 10% reduction, cracks an 18% reduction, and missing grain boundary atoms a 20% reduction. At 12% porosity, missing grain boundary atoms can create a reduction in flow stress as high as 40% [54].

Chapter 5

SUMMARY, CONCLUSIONS, AND FUTURE DIRECTIONS

In the first two chapters and the fourth chapter of this thesis, we have discussed a multitude of factors which affect the hardness and Young's Modulus of nanocrystalline materials, specifically Ni. The most obvious factor is grain size. Above the Hall-Petch breakdown ($d > 25$ nm), decreasing grain size creates an increase in strength generally described by the Hall-Petch relationship, although the value for k can be sensitive to experimental details, and we found that an exponent of -0.3 to -0.4 would be more appropriate for nanocrystalline Ni than $-1/2$ which is generally used in the Hall-Petch relationship. Young's modulus remains essentially constant with respect to grain size above the Hall-Petch breakdwon. Below the Hall-Petch breakdown ($d < 10 - 20$ nm), hardness can decrease or remain constant with decreasing grain size, and Young's modulus decreases rapidly with decreasing grain size.

However, grain size is not the only factor affecting hardness, and many deviations from the Hall-Petch relationship can be explained by other experimental factors. Addition of W to nanocrystalline Ni allows for control of grain size as well as the acheivement of finer grain sizes, but also increases hardness. Furthermore, W addition shifts the grain size at which the Hall-Petch breakdown occurs to smaller grain sizes. Annealing nanocrystalline Ni-W also increases hardness by grain boundary relaxation strengthening. Additionally, texture impacts both hardness and Young's modulus. Given that the Young's modulus for single-crystal Ni is significantly higher in the (111) direction than the (100) direction, nanocrystalline Ni with (111) texture has a higher modulus. Texture can also affect the steepness of the Hall-Petch slope, and since texture can be correlated with grain size, this can create confusing experimental results for the Hall-Petch slope. Finally, porosity decreases both hardness and Young's modulus. The shape of pores, the extent of cracking on the pores' surfaces, and how the pores impact impurity segregation all affect how dramatic is the decrease in hardness and Young's modulus.

Despite the multitude of factors which have been investigated in the literature that can create low measured values for hardness and Young's modulus, none of these factors can account for the observed values for chemically derived nanocrystalline

Ni which are two orders of magnitude lower than what is reported in the literature for nanocrystalline Ni produced by other methods. The methods commonly used in the literature to fabricate nanocrystalline Ni (electrodeposition, inert gas condensation) are very different from our method. Clearly, more research needs to be done to explain our results and determine what about chemically-derived nanocystalline Ni makes it so different from nanocrystalline Ni made from other methods.

The first step in further investigating chemically-derived nanocrystalline Ni is to gather a better understanding of the microstructure. While SEM images provide some idea of microstructure, TEM imaging would provide much more detail including a more accurate measurement of grain size, an idea of the texturing of the films, and the potential to image grain boundaries, dislocations, and other defects. Taking cross-sections of the films and imaging with SEM would allow for a measurement of porosity. Furthermore, EDS would provide information on the type, concentration, and distribution of impurities in the films.

Future work should also include further mechanical characterization. In-situ nanoindentation of films as well as imaging of indents post-indentation could allow for a better understanding how the deformation occurs. Futhermore, as mentioned in chapter 3, the same method for fabricating chemically-derived Ni could be used to additively manufacture nanoscale, nanocrystalline Ni pillars. This would allow for uniaxial compression testing which provides another way to measure elastic modulus and a way to measure strength. This future work should provide greater understanding of the microstructure and mechanical properties of new chemically-derived metals and how they compare to more traditional nanocrystalline metals.

BIBLIOGRAPHY

[1] M. A. Meyers, A. Mishra, and D. J. Benson. "Mechanical properties of nanocrystalline materials". en. In: *Progress in Materials Science* 51.4 (May 2006), pp. 427–556. ISSN: 0079-6425. DOI: 10.1016/j.pmatsci.2005.08.003. URL: http://www.sciencedirect.com/science/article/pii/S0079642505000447 (visited on 02/19/2020).

[2] E. O. Hall. "The Deformation and Ageing of Mild Steel: III Discussion of Results". en. In: *Proceedings of the Physical Society. Section B* 64.9 (Sept. 1951). Publisher: IOP Publishing, pp. 747–753. ISSN: 0370-1301. DOI: 10.1088/0370-1301/64/9/303. URL: https://doi.org/10.1088%2F0370-1301%2F64%2F9%2F303 (visited on 05/22/2020).

[3] N. J. PETCH. "The Cleavage Strength of Polycrystals". In: *Journal of the Iron and Steel Institute* 174 (1953), pp. 25–28. URL: https://ci.nii.ac.jp/naid/10019881123/ (visited on 05/22/2020).

[4] Z. C. Cordero, B. E. Knight, and C. A. Schuh. "Six decades of the Hall–Petch effect – a survey of grain-size strengthening studies on pure metals". In: *International Materials Reviews* 61.8 (Nov. 2016), pp. 495–512. ISSN: 0950-6608. DOI: 10.1080/09506608.2016.1191808. URL: https://doi.org/10.1080/09506608.2016.1191808 (visited on 02/25/2020).

[5] K. S. Kumar et al. "Deformation of electrodeposited nanocrystalline nickel". en. In: *Acta Materialia* 51.2 (Jan. 2003), pp. 387–405. ISSN: 1359-6454. DOI: 10.1016/S1359-6454(02)00421-4. URL: http://www.sciencedirect.com/science/article/pii/S1359645402004214 (visited on 02/25/2020).

[6] Zhiwei Shan et al. "Grain Boundary-Mediated Plasticity in Nanocrystalline Nickel". en. In: *Science* 305.5684 (July 2004), pp. 654–657. ISSN: 0036-8075, 1095-9203. DOI: 10.1126/science.1098741. URL: https://science.sciencemag.org/content/305/5684/654 (visited on 02/25/2020).

[7] P. M. Derlet, A. Hasnaoui, and H. Van Swygenhoven. "Atomistic simulations as guidance to experiments". en. In: *Scripta Materialia*. Viewpoint Set No. 31. Mechanical Properties of Fully Dense Nanocrystalline Metals 49.7 (Oct. 2003), pp. 629–635. ISSN: 1359-6462. DOI: 10.1016/S1359-6462(03)00400-7. URL: http://www.sciencedirect.com/science/article/pii/S1359646203004007 (visited on 05/29/2020).

[8] D. Wolf et al. "Deformation of nanocrystalline materials by molecular-dynamics simulation: relationship to experiments?" en. In: *Acta Materialia* 53.1 (Jan. 2005), pp. 1–40. ISSN: 1359-6454. DOI: 10.1016/j.actamat.2004.08.045. URL: http://www.sciencedirect.com/science/article/pii/S1359645404005087 (visited on 05/29/2020).

[9] Leon L. Shaw, Angel L. Ortiz, and Juan C. Villegas. "Hall–Petch relationship in a nanotwinned nickel alloy". en. In: *Scripta Materialia* 58.11 (June 2008), pp. 951–954. ISSN: 1359-6462. DOI: 10.1016/j.scriptamat.2008.01.025. URL: http://www.sciencedirect.com/science/article/pii/S1359646208000663 (visited on 05/23/2020).

[10] Verena Maier et al. "Nanoindentation strain-rate jump tests for determining the local strain-rate sensitivity in nanocrystalline Ni and ultrafine-grained Al". en. In: *Journal of Materials Research* 26.11 (June 2011). Publisher: Cambridge University Press, pp. 1421–1430. ISSN: 2044-5326, 0884-2914. DOI: 10.1557/jmr.2011.156. URL: https://www.cambridge.org/core/journals/journal-of-materials-research/article/nanoindentation-strainrate-jump-tests-for-determining-the-local-strainrate-sensitivity-in-nanocrystalline-ni-and-ultrafinegrained-al/FEF27CFF983709AEE2BDAB315EE82245 (visited on 03/30/2020).

[11] Tamás Kolonits et al. "Effect of bath additives on the microstructure, lattice defect density and hardness of electrodeposited nanocrystalline Ni films". en. In: *Surface and Coatings Technology* 349 (Sept. 2018), pp. 611–621. ISSN: 0257-8972. DOI: 10.1016/j.surfcoat.2018.06.052. URL: http://www.sciencedirect.com/science/article/pii/S0257897218306273 (visited on 03/30/2020).

[12] Garima Sharma et al. "Grain growth characteristics and its effect on deformation behavior in nanocrystalline Ni". en. In: *Materials Science and Engineering: A* 539 (Mar. 2012), pp. 324–329. ISSN: 09215093. DOI: 10.1016/j.msea.2012.01.102. URL: https://linkinghub.elsevier.com/retrieve/pii/S0921509312001505 (visited on 03/31/2020).

[13] Alexander Leitner, Verena Maier-Kiener, and Daniel Kiener. "Extraction of Flow Behavior and Hall–Petch Parameters Using a Nanoindentation Multiple Sharp Tip Approach". en. In: *Advanced Engineering Materials* 19.4 (2017). _eprint: https://onlinelibrary.wiley.com/doi/pdf/10.1002/adem.201600669, p. 1600669. ISSN: 1527-2648. DOI: 10.1002/adem.201600669. URL: https://onlinelibrary.wiley.com/doi/abs/10.1002/adem.201600669 (visited on 03/31/2020).

[14] R. Mishra, B. Basu, and R. Balasubramaniam. "Effect of grain size on the tribological behavior of nanocrystalline nickel". en. In: *Materials Science and Engineering: A* 373.1 (May 2004), pp. 370–373. ISSN: 0921-5093. DOI: 10.1016/j.msea.2003.09.107. URL: http://www.sciencedirect.com/science/article/pii/S0921509303015399 (visited on 05/25/2020).

[15] J.D. Giallonardo et al. "The influence of grain size and texture on the Young's modulus of nanocrystalline nickel and nickel–iron alloys". en. In: *Philosophical Magazine* 91.36 (Dec. 2011), pp. 4594–4605. ISSN: 1478-6435, 1478-6443. DOI: 10.1080/14786435.2011.615350. URL: http://www.tandfonline.com/doi/abs/10.1080/14786435.2011.615350 (visited on 04/21/2020).

[16] Liping Wang et al. “A comparative study on the tribological behavior of nanocrystalline nickel and cobalt coatings correlated with grain size and phase structure”. en. In: *Materials Chemistry and Physics* 99.1 (Sept. 2006), pp. 96–103. ISSN: 0254-0584. DOI: 10.1016/j.matchemphys.2005.10.014. URL: http://www.sciencedirect.com/science/article/pii/S0254058405007303 (visited on 05/26/2020).

[17] A. Godon et al. “Effects of grain orientation on the Hall–Petch relationship in electrodeposited nickel with nanocrystalline grains”. en. In: *Scripta Materialia* 62.6 (Mar. 2010), pp. 403–406. ISSN: 1359-6462. DOI: 10.1016/j.scriptamat.2009.11.038. URL: http://www.sciencedirect.com/science/article/pii/S1359646209007507 (visited on 05/08/2020).

[18] X. F. Zhang et al. “Influences of grain size and grain boundary segregation on mechanical behavior of nanocrystalline Ni”. en. In: *Materials Science and Engineering: A* 527.9 (Apr. 2010), pp. 2297–2304. ISSN: 0921-5093. DOI: 10.1016/j.msea.2009.12.005. URL: http://www.sciencedirect.com/science/article/pii/S092150930901291X (visited on 05/26/2020).

[19] A. M. El-Sherik et al. “Deviations from hall-petch behaviour in as-prepared nanocrystalline nickel”. en. In: *Scripta Metallurgica et Materialia* 27.9 (Nov. 1992), pp. 1185–1188. ISSN: 0956-716X. DOI: 10.1016/0956-716X(92)90596-7. URL: http://www.sciencedirect.com/science/article/pii/0956716X92905967 (visited on 05/26/2020).

[20] C. A. Schuh, T. G. Nieh, and T. Yamasaki. “Hall–Petch breakdown manifested in abrasive wear resistance of nanocrystalline nickel”. en. In: *Scripta Materialia* 46.10 (May 2002), pp. 735–740. ISSN: 1359-6462. DOI: 10.1016/S1359-6462(02)00062-3. URL: http://www.sciencedirect.com/science/article/pii/S1359646202000623 (visited on 05/26/2020).

[21] G. D. Hughes et al. “Hall-petch strengthening for the microhardness of twelve nanometer grain diameter electrodeposited nickel”. en. In: *Scripta Metallurgica* 20.1 (Jan. 1986), pp. 93–97. ISSN: 0036-9748. DOI: 10.1016/0036-9748(86)90219-X. URL: http://www.sciencedirect.com/science/article/pii/003697488690219X (visited on 05/26/2020).

[22] F Ebrahimi et al. “Mechanical properties of nanocrystalline nickel produced by electrodeposition”. en. In: *Nanostructured Materials* 11.3 (May 1999), pp. 343–350. ISSN: 0965-9773. DOI: 10.1016/S0965-9773(99)00050-1. URL: http://www.sciencedirect.com/science/article/pii/S0965977399000501 (visited on 05/26/2020).

[23] Christopher A. Schuh and T. G. Nieh. “Hardness and Abrasion Resistance of Nanocrystalline Nickel Alloys Near the Hall-Petch Breakdown Regime”. en. In: *MRS Online Proceedings Library Archive* 740 (2002). Publisher: Cambridge University Press. ISSN: 0272-9172, 1946-4274. DOI: 10.1557/PROC-740-I1.8. URL: http://www.cambridge.org/core/journals/mrs-online-proceedings-library-archive/article/hardness-

and-abrasion-resistance-of-nanocrystalline-nickel-alloys-near-the-hallpetch-breakdown-regime/84DACD5AB08C325063C7503F493E4D7D (visited on 04/14/2020).

[24] C. Ma et al. "Hardness of porous nanocrystalline Co-Ni electrodeposits". en. In: *Metals and Materials International* 19.6 (Nov. 2013), pp. 1187–1192. ISSN: 1598-9623, 2005-4149. DOI: 10.1007/s12540-013-6006-y. URL: http://link.springer.com/10.1007/s12540-013-6006-y (visited on 05/03/2020).

[25] Y. Zhou et al. "Young's modulus in nanostructured metals". In: *Zeitschrift für Metallkunde* 94.10 (Oct. 2003). Publisher: Hanser Verlag, pp. 1157–1161. ISSN: 0044-3093. DOI: 10.3139/146.031157. URL: https://www.hanser-elibrary.com/doi/abs/10.3139/146.031157 (visited on 05/09/2020).

[26] Feng Liu and Reiner Kirchheim. "Nano-scale grain growth inhibited by reducing grain boundary energy through solute segregation". en. In: *Journal of Crystal Growth* 264.1 (Mar. 2004), pp. 385–391. ISSN: 0022-0248. DOI: 10.1016/j.jcrysgro.2003.12.021. URL: http://www.sciencedirect.com/science/article/pii/S0022024803022255 (visited on 05/20/2020).

[27] Timothy J. Rupert, Jason R. Trelewicz, and Christopher A. Schuh. "Grain boundary relaxation strengthening of nanocrystalline Ni–W alloys". en. In: *Journal of Materials Research* 27.9 (May 2012). Publisher: Cambridge University Press, pp. 1285–1294. ISSN: 2044-5326, 0884-2914. DOI: 10.1557/jmr.2012.55. URL: https://www.cambridge.org/core/journals/journal-of-materials-research/article/grain-boundary-relaxation-strengthening-of-nanocrystalline-niw-alloys/DE59D72045C9D7815F0DD4F6D946B104 (visited on 03/30/2020).

[28] Isao Matsui et al. "Relationship between grain boundary relaxation strengthening and orientation in electrodeposited bulk nanocrystalline Ni alloys". en. In: *Materials Letters* 205 (Oct. 2017), pp. 211–214. ISSN: 0167577X. DOI: 10.1016/j.matlet.2017.06.094. URL: https://linkinghub.elsevier.com/retrieve/pii/S0167577X17309953 (visited on 03/31/2020).

[29] A. Giga et al. "Demonstration of an inverse Hall–Petch relationship in electrodeposited nanocrystalline Ni–W alloys through tensile testing". en. In: *Scripta Materialia* 55.2 (July 2006), pp. 143–146. ISSN: 1359-6462. DOI: 10.1016/j.scriptamat.2006.03.047. URL: http://www.sciencedirect.com/science/article/pii/S1359646206002739 (visited on 04/14/2020).

[30] C. A. Schuh, T. G. Nieh, and H. Iwasaki. "The effect of solid solution W additions on the mechanical properties of nanocrystalline Ni". en. In: *Acta Materialia* 51.2 (Jan. 2003), pp. 431–443. ISSN: 1359-6454. DOI: 10.1016/S1359-6454(02)00427-5. URL: http://www.sciencedirect.com/science/article/pii/S1359645402004275 (visited on 04/14/2020).

[31] Jason R. Trelewicz and Christopher A. Schuh. "The Hall–Petch breakdown in nanocrystalline metals: A crossover to glass-like deformation". en. In: *Acta Materialia* 55.17 (Oct. 2007), pp. 5948–5958. ISSN: 1359-6454. DOI: 10.1016/j.actamat.2007.07.020. URL: http://www.sciencedirect.com/science/article/pii/S1359645407004685 (visited on 05/07/2020).

[32] Andrew J. Detor and Christopher A. Schuh. "Tailoring and patterning the grain size of nanocrystalline alloys". en. In: *Acta Materialia* 55.1 (Jan. 2007), pp. 371–379. ISSN: 1359-6454. DOI: 10.1016/j.actamat.2006.08.032. URL: http://www.sciencedirect.com/science/article/pii/S1359645406006082 (visited on 05/08/2020).

[33] A. J. Detor, M. K. Miller, and C. A. Schuh. "Measuring grain-boundary segregation in nanocrystalline alloys: direct validation of statistical techniques using atom probe tomography". In: *Philosophical Magazine Letters* 87.8 (Aug. 2007). Publisher: Taylor & Francis _eprint: https://doi.org/10.1080/09500830701400125, pp. 581–587. ISSN: 0950-0839. DOI: 10.1080/09500830701400125. URL: https://doi.org/10.1080/09500830701400125 (visited on 05/28/2020).

[34] A. J. Detor, M. K. Miller, and C. A. Schuh. "Solute distribution in nanocrystalline Ni–W alloys examined through atom probe tomography". In: *Philosophical Magazine* 86.28 (Oct. 2006). Publisher: Taylor & Francis _eprint: https://doi.org/10.1080/14786430600726749, pp. 4459–4475. ISSN: 1478-6435. DOI: 10.1080/14786430600726749. URL: https://doi.org/10.1080/14786430600726749 (visited on 05/28/2020).

[35] *C. W. Bale, E. Bélisle, P. Chartrand, S. A. Decterov, G. Eriksson, A.E. Gheribi, K. Hack, I. H. Jung, Y. B. Kang, J. Melançon, A. D. Pelton, S. Petersen, C. Robelin. J. Sangster, P. Spencer and M-A. Van Ende, FactSage Thermochemical Software and Databases - 2010 - 2016, Calphad, vol. 54, pp 35-53, 2016 <www.factsage.com>.*

[36] Timothy J. Rupert, Jonathan C. Trenkle, and Christopher A. Schuh. "Enhanced solid solution effects on the strength of nanocrystalline alloys". en. In: *Acta Materialia* 59.4 (Feb. 2011), pp. 1619–1631. ISSN: 1359-6454. DOI: 10.1016/j.actamat.2010.11.026. URL: http://www.sciencedirect.com/science/article/pii/S1359645410007810 (visited on 05/21/2020).

[37] D. Jang and M. Atzmon. "Grain-boundary relaxation and its effect on plasticity in nanocrystalline Fe". In: *Journal of Applied Physics* 99.8 (Apr. 2006). Publisher: American Institute of Physics, p. 083504. ISSN: 0021-8979. DOI: 10.1063/1.2187417. URL: https://aip.scitation.org/doi/full/10.1063/1.2187417 (visited on 05/21/2020).

[38] S Ranganathan, R Divakar, and V. S Raghunathan. "Interface structures in nanocrystalline materials". en. In: *Scripta Materialia* 44.8 (May 2001), pp. 1169–1174. ISSN: 1359-6462. DOI: 10.1016/S1359-6462(01)00678-9. URL: http://www.sciencedirect.com/science/article/pii/S1359646201006789 (visited on 05/21/2020).

[39] X. L. Wu and Y. T Zhu. "Partial-dislocation-mediated processes in nanocrystalline Ni with nonequilibrium grain boundaries". In: *Applied Physics Letters* 89.3 (July 2006). Publisher: American Institute of Physics, p. 031922. ISSN: 0003-6951. DOI: 10.1063/1.2227639. URL: https://aip.scitation.org/doi/full/10.1063/1.2227639 (visited on 05/21/2020).

[40] Jörg Löffler and Jörg Weissmüller. "Grain-boundary atomic structure in nanocrystalline palladium from x-ray atomic distribution functions". In: *Physical Review B* 52.10 (Sept. 1995). Publisher: American Physical Society, pp. 7076–7093. DOI: 10.1103/PhysRevB.52.7076. URL: https://link.aps.org/doi/10.1103/PhysRevB.52.7076 (visited on 05/21/2020).

[41] A.J. Detor and C.A. Schuh. "Microstructural evolution during the heat treatment of nanocrystalline alloys". en. In: *Journal of Materials Research* 22.11 (Nov. 2007), pp. 3233–3248. ISSN: 0884-2914, 2044-5326. DOI: 10.1557/JMR.2007.0403. URL: https://www.cambridge.org/core/product/identifier/S0884291400026765/type/journal_article (visited on 05/21/2020).

[42] J. Amblard et al. "Inhibition and nickel electrocrystallization". en. In: *Journal of Applied Electrochemistry* 9.2 (Mar. 1979), pp. 233–242. ISSN: 1572-8838. DOI: 10.1007/BF00616093. URL: https://doi.org/10.1007/BF00616093 (visited on 05/21/2020).

[43] Daryl W. Yee et al. "Additive Manufacturing of 3D-Architected Multifunctional Metal Oxides". en. In: *Advanced Materials* 31.33 (2019), p. 1901345. ISSN: 1521-4095. DOI: 10.1002/adma.201901345. URL: https://onlinelibrary.wiley.com/doi/abs/10.1002/adma.201901345 (visited on 02/18/2020).

[44] W. C. Oliver and G. M. Pharr. "An improved technique for determining hardness and elastic modulus using load and displacement sensing indentation experiments". en. In: *Journal of Materials Research* 7.6 (June 1992), pp. 1564–1583. ISSN: 2044-5326, 0884-2914. DOI: 10.1557/JMR.1992.1564. URL: http://www.cambridge.org/core/journals/journal-of-materials-research/article/an-improved-technique-for-determining-hardness-and-elastic-modulus-using-load-and-displacement-sensing-indentation-experiments/A53D45298E14F73B86495BBC056E16 (visited on 05/08/2020).

[45] G. W. Nieman, J. R. Weertman, and R. W. Siegel. "Mechanical behavior of nanocrystalline Cu and Pd". en. In: *Journal of Materials Research* 6.5 (May 1991). Publisher: Cambridge University Press, pp. 1012–1027. ISSN: 2044-5326, 0884-2914. DOI: 10.1557/JMR.1991.1012. URL: http://www.cambridge.org/core/journals/journal-of-materials-research/article/mechanical-behavior-of-nanocrystalline-cu-and-pd/F26FB300A849F42702858323315CCDF9 (visited on 04/30/2020).

[46] Shi-Jin Zhao, Karsten Albe, and Horst Hahn. “Grain size dependence of the bulk modulus of nanocrystalline nickel”. en. In: *Scripta Materialia* 55.5 (Sept. 2006), pp. 473–476. ISSN: 1359-6462. DOI: 10.1016/j.scriptamat.2006.04.043. URL: http://www.sciencedirect.com/science/article/pii/S1359646206003538 (visited on 05/29/2020).

[47] V. Krstic, U. Erb, and G. Palumbo. “Effect of porosity on Young’s modulus of nanocrystalline materials”. en. In: *Scripta Metallurgica et Materialia* 29.11 (Dec. 1993), pp. 1501–1504. ISSN: 0956-716X. DOI: 10.1016/0956-716X(93)90344-R. URL: http://www.sciencedirect.com/science/article/pii/0956716X9390344R (visited on 04/23/2020).

[48] D. C. Hurley et al. “Anisotropic elastic properties of nanocrystalline nickel thin films”. en. In: *Journal of Materials Research* 20.5 (May 2005). Publisher: Cambridge University Press, pp. 1186–1193. ISSN: 2044-5326, 0884-2914. DOI: 10.1557/JMR.2005.0146. URL: https://www.cambridge.org/core/journals/journal-of-materials-research/article/anisotropic-elastic-properties-of-nanocrystalline-nickel-thin-films/052EF27FFA7180811D60D2BD7972E6E8 (visited on 04/23/2020).

[49] T. Fritz et al. “Determination of Young’s modulus of electroplated nickel”. en. In: *Electrochimica Acta*. Electrochemistry in Molecular and Microscopic Dimensions 48.20 (Sept. 2003), pp. 3029–3035. ISSN: 0013-4686. DOI: 10.1016/S0013-4686(03)00370-0. URL: http://www.sciencedirect.com/science/article/pii/S0013468603003700 (visited on 05/18/2020).

[50] Anna Torrents, Heather Yang, and Farghalli A. Mohamed. “Effect of Annealing on Hardness and the Modulus of Elasticity in Bulk Nanocrystalline Nickel”. en. In: *Metallurgical and Materials Transactions A* 41.3 (Mar. 2010), pp. 621–630. ISSN: 1543-1940. DOI: 10.1007/s11661-009-0147-0. URL: https://doi.org/10.1007/s11661-009-0147-0 (visited on 05/18/2020).

[51] J. de Klerk and M. J. P. Musgrave. “Internal Conical Refraction of Transverse Elastic Waves in a Cubic Crystal”. en. In: *Proceedings of the Physical Society. Section B* 68.2 (Feb. 1955). Publisher: IOP Publishing, pp. 81–88. ISSN: 0370-1301. DOI: 10.1088/0370-1301/68/2/303. URL: https://doi.org/10.1088%2F0370-1301%2F68%2F2%2F303 (visited on 05/19/2020).

[52] James C. M. Li. “Grain boundary impurity and porosity effects on the yield strength of nanocrystalline materials”. In: *Applied Physics Letters* 90.4 (Jan. 2007). Publisher: American Institute of Physics, p. 041912. ISSN: 0003-6951. DOI: 10.1063/1.2430491. URL: https://aip.scitation.org/doi/10.1063/1.2430491 (visited on 05/03/2020).

[53] James C. M. Li. “Mechanical Grain Growth in Nanocrystalline Copper”. In: *Physical Review Letters* 96.21 (June 2006). Publisher: American Physical Society, p. 215506. DOI: 10.1103/PhysRevLett.96.215506. URL: https:

//link.aps.org/doi/10.1103/PhysRevLett.96.215506 (visited on 05/20/2020).

[54] J. Schiøtz et al. “Atomic-scale simulations of the mechanical deformation of nanocrystalline metals”. In: *Physical Review B* 60.17 (Nov. 1999). Publisher: American Physical Society, pp. 11971–11983. DOI: 10.1103/PhysRevB.60.11971. URL: https://link.aps.org/doi/10.1103/PhysRevB.60.11971 (visited on 05/03/2020).